Draft version September 10, 2025
Typeset using LaTeX **manuscript** style in AASTeX7.0.1

Balmer Absorption in Iron Low-Ionization Broad Absorption Line Quasars

Karen M. Leighly,[1] Sarah C. Gallagher,[2,3] Hyunseop Choi,[4] Donald M. Terndrup,[1,5] Julianna R. Voelker,[1] Gordon T. Richards,[6] and Leah K. Morabito[7,8]

[1]*Homer L. Dodge Department of Physics and Astronomy, The University of Oklahoma, 440 W. Brooks St., Norman, OK 73019, USA*

[2]*Department of Physics & Astronomy, The University of Western Ontario, London, ON, N6A 3K7, Canada*

[3]*Institute for Earth and Space Exploration, The University of Western Ontario, London, ON, N6A 3K7, Canada*

[4]*Département de Physique, Université de Montréal, Succ. Centre-Ville, Montréal, Québec, H3C 3J7, Canada*

[5]*Department of Astronomy, The Ohio State University, 140 W. 18th Ave., Columbus, OH 43210, USA*

[6]*Department of Physics, Drexel University, 32 S. 32nd St., Philadelphia, PA 19104, USA*

[7]*Centre for Extragalactic Astronomy, Department of Physics, Durham University, Durham DH1 3LE, UK*

[8]*Institute for Computational Cosmology, Department of Physics, Durham University, Durham DH1 3LE, UK*

ABSTRACT

While C IV is the most common absorption line in Broad Absorption Line Quasar spectra, Balmer absorption lines are among the rarest. We present analysis of Balmer absorption in a sample of fourteen iron low-ionization BAL quasars (FeLoBALQs); eight are new identifications. We measured velocity offset, width, and apparent optical depth. The partial covering ubiquitous in BAL quasar spectra alters the measured Balmer optical depth ratios; taking that into account, we estimated the true H($n = 2$) column density. We found the anticipated correlation between Eddington ratio and outflow speed, but it is weak in this sample because nearly all of the objects have the low outflow speeds characterizing loitering outflow FeLoBAL quasars (H. Choi et al. 2022b), objects that are also found to have low accretion rates (K. M. Leighly et al.

Email: leighly@ou.edu

2022; H. Choi et al. 2022a). Measures of dN/dv, the differential column density with respect to the outflow speed, are anticorrelated with the luminosity and Eddington ratio: the strongest absorption is observed at the lowest speeds in the lowest luminosity objects. The absorption line width is correlated with α_{oi}, the F_λ point-to-point slope between 5100Å and 3μm. This parameter is strongly correlated with the Eddington ratio among low-redshift quasars (K. M. Leighly et al. 2024). Balmer absorption lines have been recently found in the spectra of Little Red Dots (LRDs), a class of high-redshift objects discovered by JWST. We note suggestive similarities between LRDs and FeLoBAL quasars in the emission line shape, the presence of steep reddening and a scattered blue continuum, the lack of hot dust emission, and X-ray weakness.

Keywords: Broad-absorption-line quasar (183), Quasars (1319)

1. INTRODUCTION

Broad absorption lines are found in about 10–26% of optically selected quasars (A. Tolea et al. 2002; P. C. Hewett & C. B. Foltz 2003; T. A. Reichard et al. 2003; J. R. Trump et al. 2006; C. Knigge et al. 2008; R. R. Gibson et al. 2009b). The absorption lines are sometimes very broad, with velocity widths of up to $10,000\,\mathrm{km\,s^{-1}}$ and strongly blueshifted (e.g., A. Baskin et al. 2015) indicating outflow velocities that sometimes exceed $0.1c$. Broad absorption line quasars (BALQs) are classified according to the lines that appear in their rest-UV spectra. High-ionization BALQs show absorption from C IV, N V, O VI, and Lyα; depending on the column density and ionization parameter of the outflow, they can also have Si IV, S IV, and P V in their spectra. Low-ionziation BALQs (LoBALQs) have all of these lines, as well as Mg II and Al III. The presence of these lines indicates that the column density of the outflow nearly reaches the hydrogen ionization front. Finally, iron low-ionization BALQs (FeLoBALQs) have all of those lines as well as absorption from Fe II.

Recently, we used the novel spectral synthesis code `SimBAL` (K. M. Leighly et al. 2022) to analyze a sample of 50 low-redshift FeLoBAL quasars (H. Choi et al. 2022b), increasing the number of well-studied FeLoBALQs in the literature by a factor of five. Although they are rare, comprising only

about 0.3% of optically selected quasars (J. R. Trump et al. 2006), FeLoBAL quasars have the highest column densities among BAL quasars and can drive some of the most massive and energetic quasar winds observed (e.g., H. Choi et al. 2020). These quasars also typically show reddened spectral energy distributions, which, together with their powerful winds, suggest that they may represent a transitionary "blow-out" evolutionary stage, during which a quasar actively expels gas and dust, transforming from a heavily shrouded ultraluminous, infrared galaxy-type (ULIRG) object to a blue quasar (e.g., D. Farrah et al. 2012). We found that the outflows lie at a large range of distances from the central engine, from 1 pc (near the torus), to kiloparsecs (in the host galaxy) (H. Choi et al. 2022b). We found that the accretion rate distribution of FeLoBAL quasars is roughly bimodal, with a low accretion rate branch centered at $L_{\rm Bol}/L_{\rm Edd} \sim -1.0$ and a high accretion rate branch with $L_{\rm Bol}/L_{\rm Edd} \sim 0.0$; in contrast, the accretion rate distribution of an unabsorbed comparison sample is strongly peaked at $L_{\rm Bol}/L_{\rm Edd} \sim -0.5$ (K. M. Leighly et al. 2022). We found that the outflow properties are linked to the accretion rate. For high accretion rate objects, the outflow speed[9] decreases with radius as expected in radiative acceleration scenarios because the radiation intensity is largest near the central engine. However, H. Choi et al. (2022b) found significant population of outliers from this relationship. Called loitering outflow FeLoBAL quasars, they are characterized by low outflow velocity ($|V_{\rm off}| < 2000\,{\rm km\,s^{-1}}$), and location near the central engine ($\log R < 1$ [pc]); we note that the class includes objects where the gas is inflowing. Loitering outflow FeLoBAL quasars are also characterized by low accretion rates (K. M. Leighly et al. 2022; H. Choi et al. 2022a). Finally, the photometry and near-IR variability properties were analyzed; notably, we found evidence that the spectral energy distributions of the loitering outflow FeLoBAL quasars show little evidence for reddening and a lack of hot dust emission (K. M. Leighly et al. 2024). The results from these four papers yielded ample evidence that low-redshift FeLoBALQs are distinct from unabsorbed objects, prompting development of a scenario for their character and evolution whereby the high-accretion-rate FeLoBAL quasars are radiating powerfully enough to drive a thick, high-velocity outflow, quasars

[9] Throughout this paper, we use the convention that outflow velocities are negative in sign, and the magnitude of the velocity is referenced as the speed.

with intermediate accretion rates may have an outflow, but it is not sufficiently thick to include Fe II absorption, and low accretion-rate FeLoBAL outflows originate in absorption in a failing torus, no longer optically thick enough to reprocess radiation into the near-IR (K. M. Leighly et al. 2024).

Recently, JWST has revealed a specific class of low-luminosity high-redshift object that are different from high-redshift quasars. Little Red Dots (LRDs) are found to have peculiar V-shaped spectra, red in the rest-frame optical band, and blue in the near-UV band. Many of these objects are thought to be Active Galactic Nuclei (AGN), as they have broad Balmer emission lines. A number of LRDs show narrow and mildly blueshifted Balmer absorption lines (e.g., F. D'Eugenio et al. 2025; D. D. Kocevski et al. 2025; J. Matthee et al. 2024); the fraction of objects with these lines may be as large as 20% (e.g., K. Inayoshi & R. Maiolino 2025).

BAL quasars are another class of extragalactic object that has occasionally been found to have Balmer line absorption. Most of these objects are FeLoBAL quasars (P. B. Hall et al. 2002; K. Aoki et al. 2006; K. Aoki 2010; S. Zhang et al. 2015; A. Schulze et al. 2018), although there are some reports of weak absorption in spectra from non-BAL quasars when the signal-to-noise ratio is excellent (J. B. Hutchings et al. 2002; T. Wang et al. 2008; T. Ji et al. 2012; J. Wang & D. W. Xu 2015). In a photoionized gas, Balmer absorption requires fairly extreme conditions including a high density (e.g., K. M. Leighly et al. 2011), high column density, and high ionization parameter, all of which work together to keep the hydrogen $n = 2$ population elevated enough to yield observable absorption. Given that FeLoBAL quasars show the highest absorption column densities among BAL quasars, it is not surprising that they show the largest equivalent Balmer absorption lines. In fact, H. Choi et al. (2022b) used the `SimBAL` results to predict which of their sample of low-redshift FeLoBALs should have Balmer absorption lines (Fig. 16 in that paper).

To follow up our results of analysis of low-redshift FeLoBAL quasars, we have initiated a project to perform `SimBAL` analysis on a sample of high-redshift objects (Choi et al. in prep.). At the same time, we are performing near-infrared spectroscopic observations using Gemini GNIRS and APO Triplespec to see if the differences found in the rest-frame optical spectra of low-redshift FeLoBALQs (K. M. Leighly et al. 2022) carry over to their more luminous high-redshift brethren. In this paper,

we present nine of our new observations with Balmer absorption in their spectra. We supplement the sample with two spectra from the literature (A. Schulze et al. 2018), and one from the Gemini archive for a set of 12 objects that have Hα absorption detected in their band pass. We also include two from H. Choi et al. (2022b); K. M. Leighly et al. (2022) that have Hβ absorption but lack NIR spectra required to view Hα. The final sample comprisies 14 objects.

§2 describes the sample and extraction of the spectra. §3 discusses the spectral fitting and extraction of parameters. §4 includes the correlation analysis. §5 discusses what we can learn about the physical properties of FeLoBAL quasar absorption from the results, and it also compares FeLoBAL quasar properties with those of LRDs. It turns out that there are similarities in the emission lines and in the spectral energy distribution, including the lack of hot dust emission, the extreme reddening and blue emission, and lack of X-ray emission. §6 summarizes the results. Throughout we use typical cosmological parameters ($H_0 = 69.32\,\mathrm{km\,Mpc^{-1}\,s^{-1}}$, $\Omega_c = 0.233$, $\Omega_\Lambda = 0.721$).

2. THE SAMPLE

FeLoBAL quasars can be studied in ground-based optical spectra for redshifts less than about 3 due to the plethora of Fe II absorption lines produced in the ionized gas. We are performing `SimBAL` analysis on a sample of $\sim$ 50 high redshift quasars (J. Voelker et al. 2021, Choi et al. in prep.); this sample has bolometric luminosities about 1 dex higher than our previously-studied low-redshift sample (median $\log L_{\rm Bol} \sim 47.1$ versus 46.2 [erg s^{-1}]) described in H. Choi et al. (2022b,a); K. M. Leighly et al. (2022, 2024). Depending on the redshift, the Hβ / Fe II / [O III] spectral region can fall in the near-infrared bands accessible from the ground; specifically, for $1.3 < z < 1.6$, this region falls in the J band, and for $2.1 < z < 2.6$, it falls in the H band. Given what we learned about FeLoBAL quasars from the low redshift sample, we targeted objects that had a wide range of Fe II morphologies, including objects with a moderate amount of excited state Fe II (e.g., A. B. Lucy et al. 2014), overlapping trough quasars (e.g., P. B. Hall et al. 2002), and the loitering outflow FeLoBALQs, characterized by very high excitation Fe II lines but low outflow velocities first identified by H. Choi et al. (2022b). We performed observations using TripleSpec (J. C. Wilson et al. 2004) on the Astrophysical Research Consortium (ARC) 3.5 meter telescope, and using GNIRS (J. H. Elias

et al. 2006a,b) on the Gemini North telescope. Two spectra were published by A. Schulze et al. (2018). A few spectra were obtained from the Gemini archive.

From the full sample of more than thirty objects, twelve included Balmer absorption in their spectra (Table 1). We also include two objects previously presented in H. Choi et al. (2022b) and K. M. Leighly et al. (2022); we present analysis of their Balmer absorption lines here. The analysis of the full sample, and well as the `SimBAL` analysis, focusing principally on the Fe II absorption in the UV band, will be presented elsewhere (Leighly et al. in prep., Choi et al. in prep.)

The Gemini GNRIS data were reduced using `PypeIt` (J. Prochaska et al. 2020). The APO TripleSpec data were reduced using `TripleSpecTool`, a modification of `SpexTool` (M. C. Cushing et al. 2004; W. D. Vacca et al. 2003).

Of our fourteen objects, six were already known to have Balmer absorption (Table 1), and eight are new detections, having never been observed in the NIR before. Several other FeLoBALQs are known to have Balmer absorption, including SDSS J125942.80+121312.6 ($z = 0.748$, P. B. Hall 2007) and SDSS J152350.42+391405.2 ($z = 0.661$, S. Zhang et al. 2015). SDSS J122826.79+100532.2 has Balmer absorption, and may have low-covering-fraction FeLoBAL absorption (G. Li et al. 2021). Objects that are not FeLoBAL quasars have been found to have Balmer absorption, but generally it is very weak and would be difficult to detect without the presented excellent signal-to-noise ratio spectra. These include SDSS J102839.11+450009.4 ($z = 0.583$, T. Wang et al. 2008), LBQS 1206+1052 ($z = 0.395$, T. Ji et al. 2012), NGC 4151($z = 0.0034$, J. B. Hutchings et al. 2002), and SDSS J112611.63+425246 (z=0.156, J. Wang & D. W. Xu 2015). A difference between our investigation and these examples is that while their discoveries were serendipious and limited to analysis of one or two objects, our target choices were predicated by our experience with FeLoBAL spectra, and our analysis focuses on the properties of the population.

Continuum properties were measured from archival photometry of the objects. For the observed frame optical band, we compiled SDSS (M. R. Blanton et al. 2017) and Pan-STARRS (K. C. Chambers et al. 2016) photometry, prioritizing Pan-STARRS when available. For the observed frame near-infrared band, we compiled 2MASS (M. F. Skrutskie et al. 2006) and UKIDSS (A. Lawrence

et al. 2007) photometry, prioritizing UKIDSS photometry when available. Seven objects did not have archival near-IR photometry. All objects had WISE photometry (E. L. Wright et al. 2010).

The spectra and photometry were corrected for Galactic reddening using the J. A. Cardelli et al. (1988) extinction curves. We had only SDSS spectra for two of the objects (SDSS 1125+0029 and SDSS 1644+5307); their redshifts were estimated using [O II] (H. Choi et al. 2022b). Redshift estimation for higher luminosity objects is a challenge since even low-ionization lines that make the best redshift indicators show evidence for outflows (e.g. N. L. Zakamska & J. E. Greene 2014). For the remaining 12 objects, we uniformly used the peak value of Hα for consistency.

Table 1. Sample

SDSS Object Name	Redshift [a]	H magnitude[b]	Telescope & Instrument	Date Observed[c]	Exposure Time (seconds)	Data Identifier	Reference[d]
080202.69+140315.1	2.143	16.05	Gemini GNIRS	2023-Nov-04	3096.0	GN-2023B-Q-239-39	···
083942.11+380526.4	2.318	16.28	Gemini GNIRS	2023-Oct-29	3096.0	GN-2023B-Q-239-48	Aoki 2006
085910.40+423911.3	1.497	15.38	Palomar 200 inch / Triplespec	···	···	···	Schulze et al. 2018
101927.37+022521.3	1.364	15.22	Palomar 200 inch / Triplespec	···	···	···	Schulze et al. 2018
112526.12+002901.3	0.8636	16.22	SDSS	···	···	···	Hall et al. 2002
122933.32+262131.2	2.581	16.09	ARC 3.5 TripleSpec	2021-Feb-24	7680.0	···	···
124452.49+583427.6	2.282	16.9[e]	Gemini GNIRS	2024-Feb-21	6192.0	GN-2024A-Q-142-23	···
143916.28+162858.5	2.218	16.6[e]	Gemini GNIRS	2023-Jul-16	2880.0	GN-2023A-Q-230-31	···
160915.16+561943.2	1.33	16.6[e]	Gemini GNIRS	2023-Jun-30	3840.0	GN-2023A-Q-230-62	···
162119.22+081950.7	2.572	17.0[e]	Gemini GNIRS	2022-Sep-10	4800.0	GN-2022A-Q-327-46	···
162527.73+093332.8	2.290	16.35	Gemini GNIRS	2024-Feb-22	2048.0	GN-2024A-Q-142-32	···
163515.87+143925.9	1.317	16.8[e]	Gemini GNIRS	2022-Sep-03	3840.0	GN-2022A-Q-237-153	···
164419.75+530750.4	0.7813	16.18	SDSS	···	···	···	Leighly et al. 2022
172341.08+555340.5	2.108	15.30	Gemini GNIRS	2023-Jun-24	960.0	GN-2023A-Q-103-53	Aoki 2010

[a] The redshifts were estimated by us from the peak of the Hα line when present; the source of the redshifts for the two SDSS spectra is given in H. Choi et al. (2022b).

[b] The infrared magnitudes listed are from 2MASS (M. F. Skrutskie et al. 2006) or UKIDSS (A. Lawrence et al. 2007), except when noted.

[c] The information is given only for spectra that we reduced; the remainder are publicly available in already-reduced form.

[d] The reference that reported the discovery of Balmer absorption.

[e] The H magnitude values were estimated by interpolation between optical (SDSS or PanSTARRS) and WISE values.

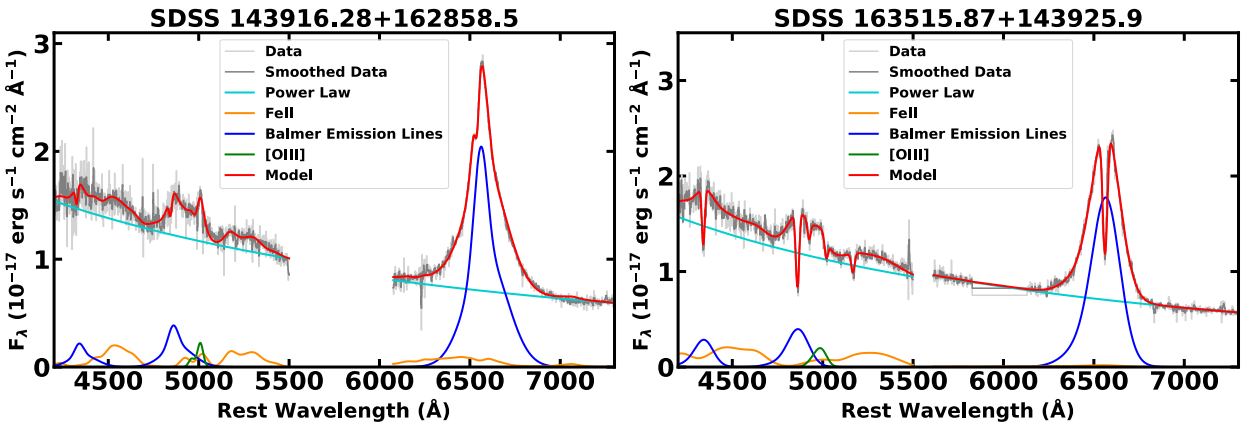

Figure 1. Examples of the spectra and model fits for two of the fourteen spectra; the remainder are found in the online journal. We note that although the flux density units are given, the spectra are not reliably flux calibrated. *Left:* SDSS 1439+1628, the object with the lowest optical depth Hα Balmer absorption line. *Right:* SDSS 1635+1439, the object with the largest optical depth Hα Balmer absorption line. The complete figure set (14 images) is available in the online journal.

3. DATA ANALYSIS

The spectra were analyzed using `Sherpa` (A. Siemiginowska et al. 2024). The spectral analysis was hampered by the wide range of signal-to-noise ratios (SNR) of the spectra (Fig. 1), due to both the low flux of the objects, and the atmospheric absorption features in the near-infrared spectra. As outlined below, a simplified model and a uniform approach was used in order to obtain the same information from each spectrum regardless of the spectral SNR. An example of two of the spectra and model fits are shown in Fig. 1, and the plots of the remainder of the spectra are given in the online journal.

Fig. Set 1. Spectra and Model fits

The continuum was modeled using a power law. The Hα and Hβ regions of the spectra were modeled with separate power laws. The Hα region was modeled typically between rest-frame 6000 and 7400Å. A Lorenzian profile adequately modeled the Balmer emission lines in most cases, although two or three Gaussian profiles were used when the line showed asymmetry. The Hα emission lines were strong and broad, and [N II], if present, was too weak to be detected. Low-level Fe II emission is observed shortward of Hα (e.g., M.-P. Véron-Cetty et al. 2004); a model constructed using the

Fe II line measurements from M.-P. Véron-Cetty et al. (2004) was used, with the width of the lines set equal to the Balmer Lorentzian width or the narrower of the two Gaussians (e.g., T. A. Boroson & R. F. Green 1992).

The Hβ region was modeled between rest-frame 4200 and 5500Å, and it was fit simultaneously with the Hα region. Both Hβ and Hγ were modeled, although in two cases, the Hγ region of the spectrum could not be fit due to poor SNR. The widths of these Balmer emission lines were constrained to be equal to the Hα line. The J. Kovačević et al. (2010) Fe II model was used, and again the width of the Fe II lines was tied to the Balmer line widths as described above.

The [O III] emission feature was modeled with one or two Gaussians depending on the spectrum; in some cases, [O III] was not observed in the spectrum, and the feature was not modeled. As usual, the two [O III] components were constrained according to atomic physics and their common kinematics.

The Balmer absorption lines were modeled using a Gaussian opacity profile, and this model provided an excellent fit. In most cases, one component was sufficient; for three objects (SDSS 1125+0029, SDSS 1244+5834, SDSS 1609+5619) two components were used. We acknowledge that the assumption of a Gaussian opacity profile may obscure more complicated kinematics; however, we felt that a simple model provided a fair treatment of all the spectra regardless of signal-to-noise ratio. Generally, we modeled Hα, Hβ, and Hγ except in the cases where the spectrum did not include the relevant bandpass or where the spectrum was exceptionally noisy. While the positions and widths of the lines were constrained according to atomic physics, our first model did not constrain the optical depth ratios. This model is referred to henceforth as the "unconstrained" model.

Table 2. Spectral Fitting Results

Object Name	Unconstrained Model					Constrained Model		Partial Covering Model	
	FWHM (km s^{-1})	Velocity Offset[a] (km s^{-1})	Hα $\tau_{\rm max}$	Hβ $\tau_{\rm max}$	Hα Apparent Column Density (10^{13} cm^{-2})	Statistically Necessary Line	True Column Density (10^{13} cm^{-2})	Best Partial Covering Model[c]	Covering Fraction[b]
080202.69+140315.1	1064 ± 16	-1360 ± 5	0.367 ± 0.005	0.128 ± 0.006	3.72 ± 0.08	Hα	3.78 ± 0.08	···	···
083942.11+380526.4	539 ± 7	-237 ± 2.4	0.634 ± 0.007	0.401 ± 0.007	3.26 ± 0.05	Hβ	14.9 ± 0.3	FC+PL	···
085910.40+423911.3	630^{+35}_{-33}	780 ± 11	0.37 ± 0.014	0.46 ± 0.07	2.23 ± 0.17	Hα	2.11 ± 0.14	···	···
101927.37+022521.3	1220^{+47}_{-51}	-1520 ± 23	0.57 ± 0.03	$0.47^{+0.13}_{-0.12}$	6.6 ± 0.4	Hα	6.6 ± 0.4	···	···
112526.12+002901.3[de]	820^{+64}_{-600}	430 ± 45	···	0.31 ± 0.03	···	Hγ	11.3 ± 2.5	PC	$0.45^{+0.09}_{-0.06}$
122933.32+583427.6	970^{+74}_{-69}	-1020 ± 30	0.33 ± 0.02	0.021 ± 0.04	3.0 ± 0.3	Hα	3.1 ± 0.3	···	···
124452.49+583427.6[e]	1330 ± 9	-1720 ± 4	0.435 ± 0.006	0.287 ± 0.005	5.02 ± 0.05	Hβ	21.2 ± 0.4	FC+PL	···
143916.28+162858.5	1127^{+30}_{-32}	-1170 ± 11	0.185 ± 0.005	0.12 ± 0.015	1.99 ± 0.08	Hα	1.86 ± 0.07	FC+PL	···
160915.16+561943.2[e]	530 ± 19	-1460 ± 14	0.56 ± 0.01	0.25 ± 0.01	4.0 ± 0.12	Hβ	15.9 ± 0.8	FC+PL	···
162119.22+081950.7	1410 ± 41	-4130 ± 20	0.247 ± 0.007	0.043 ± 0.008	3.33 ± 0.13	Hα	3.33 ± 0.13	···	···
162527.73+093332.8	1010 ± 110	-6620 ± 13	0.27 ± 0.01	0.143 ± 0.009	2.5 ± 0.3	Hα	2.5 ± 0.34	···	···
163515.87+143925.9	1235^{+11}_{-15}	-140 ± 5	0.745 ± 0.006	0.66 ± 0.012	8.8 ± 0.1	Hγ	96 ± 4	FC+PL	···
164419.75+530750.4[d]	820 ± 40	-1560 ± 13	···	0.40 ± 0.02	···	Hγ	14.0 ± 1.2	PC	$0.31^{+0.007}_{-0.025}$
172341.08+555340.5[f]	1085^{+17}_{-16}	-5500 ± 6.4	0.47 ± 0.01	0.243 ± 0.006	4.9 ± 0.13	Hγ	12.1 ± 0.4	P(L+C)	0.21 ± 0.004

Table 2 *continued on next page*

Table 2 *(continued)*

Object Name	Unconstrained Model					Constrained Model		Partial Covering Model	
	FWHM (km s^{-1})	Velocity Offset[a] (km s^{-1})	Hα $\tau_{\rm max}$	Hβ $\tau_{\rm max}$	Hα Apparent Column Density (10^{13} cm^{-2})	Statistically Necessary Line	True Column Density (10^{13} cm^{-2})	Best Partial Covering Model[c]	Covering Fraction[b]

[a] All of the objects meet the velocity criterion identifying a loitering outflow FeLoBAL quasar ($|V_{\rm off}| < 2000\,{\rm km\,s^{-1}}$) except SDSS J1621+0819, SDSS J1625+0933, and SDSS J1723+5553. Of these, only SDSS J1723+5553 lacks the strong very highly excited Fe II absorption around 2500Å that signals a location near the torus (e.g., Fig. 3 H. Choi et al. 2022b).

[b] The step-function partial covering fraction in the case where the continuum is partially covered. If the continuum is fully covered, the covering fraction is assumed to be 1.

[c] No entry: the Balmer optical depth line ratios are statistically consistent with the values required by atomic physics, and no partial covering is necessary. P(L+C): partial covering of both the emission lines and the continuum; FC+PL: full covering of the continuum, partial covering of the emission lines; PC: partial covering of the continuum, emission lines are not covered.

[d] The spectra of these objects do not include Hα in the bandpass.

[e] These objects required two Gaussian components to model the Balmer absorption lines. The FWHM measurements are for the two-component feature, and the τ-weighted velocity offset is given.

[f] As noted by K. Aoki (2010), in this object the Hα absorption line falls upon a prominent CO telluric feature, making the measurement of depth uncertain.

The results are given in Table 2. We report the FWHM of the absorption feature and the optical depth (normalization). For single features, the uncertainties were taken from the `Sherpa` models. In the several cases where there were two components, we measured the FWHM and optical depth normalization from the combined profile. The uncertainties were generated by simulating 10000 profiles with parameters drawn from normal distributions given by the `Sherpa` best fit and errors. The 1σ errors on the full profile were obtained from the distribution of measurements from the simulated profiles. We also report the apparent hydrogen column density in $n = 2$ from the Hα profile. These were computed in the usual way from B. D. Savage & K. R. Sembach (1991, Equation 9). This can be regarded as a lower limit to the column density, since it does not take into account partial covering.

3.1. *Partial Covering*

It is well known that quasar absorption often exhibits partial covering, i.e., the absorbing outflow does not completely occult the continuum emission region (e.g., see K. M. Leighly et al. 2019, for references and discussion). Partial covering is recognized in the spectra presented in this paper through comparison of the optical depths of the different Balmer lines. Atomic physics requires that τ_1/τ_2 equals the ratio of the products of the line wavelength and oscillator strength (e.g., B. D. Savage & K. R. Sembach 1991). In our case, the ratio of Hβ to Hα optical depths should be 0.14, while the ratio of Hγ to Hβ should be 0.33. In nearly all cases, the best-fitting optical depths (Table 2) gave ratios larger than these values, indicating the presence of partial covering, but not the statistical necessity of partial covering. Thus, our second set of model fits constrained the relative optical depths to be the values demanded by atomic physics. We then compared the χ^2 for the constrained and unconstrained models using the F-test. We found that the spectra of six objects were consistent with no partial covering (Table 2). These objects had either very noisy spectra or very low optical depth absorption (Fig. 1.).

The nature of partial covering is a complex subject; see K. M. Leighly et al. (2019) for a discussion. Given the fact that we are constraining partial covering using only two or three lines, we used step-function partial covering (e.g., N. Arav et al. 2005) as the simplest model. In this model, the absorber

uniformly occults a fraction of the continuum emission region given by c_f, while the remainder is not occulted. This model is complicated by the fact that the continuum and the broad line region may have different covering fractions (e.g., R. Ganguly et al. 1999).

Given the limits of the data, we adopt the following spectral-fitting strategy to obtain an estimate of the true column density. Since partial covering is present, the apparent optical depth of Hα yields only a lower limit of the column density of neutral hydrogen in $n = 2$. As discussed above, partial covering is recognized in data when the ratio of a weaker to stronger line is larger than predicted by atomic physics. Therefore, the higher order lines yield higher (i.e., better) lower limits. So we use the F test to determine the smallest statistically necessary Balmer line[10]. These are listed in Table 2. Another approach would have been to report the optical depth from the best-fitting partial covering model. However, given the range of signal-to-noise ratios exhibited by the spectra, that result would have been model dependent. Cleaving closely to measurements obtained directly from the data provides a more model-independent approach.

The covering fraction can be obtained directly from the optical depth ratios (e.g. R. Ganguly et al. 1999; B. M. Sabra & F. Hamann 2001; N. Arav et al. 2005), but in that case, estimating the uncertainty in the covering fractions may not be straightforward. Instead, we use the flexibility of `Sherpa` to construct an analytical partial covering model.

The true column density is equal to the observed column density times the covering fraction (e.g., N. Arav et al. 2005). Also, in principle, the continuum covering fraction and emission line covering fraction can be measured separately (e.g., R. Ganguly et al. 1999). But given the SNR limitations of our spectra, we consider three limiting partial covering scenarios. In all of these, the higher order Balmer line optical depths are constrained according to atomic physics, i.e., using the ratios given above.

[10] For example, we compared the χ^2 for a model with Hα, Hβ, and Hγ with the χ^2 for a model including only Hα and Hβ. If the F test indicates that Hγ is statistically necessary, it is the smallest statistically necessary line, and the column density is determined from it. If not, we repeat the test with Hβ, and so on.

1. **P(C+L):** The absorber partially covers both the continuum and the emission line region. The true column density is the product of the covering fraction times the column density estimated from the smallest statistically necessary line.

2. **PC:** The absorber partially covers the continuum emitting region, leaving the emission-line region uncovered. The true column density is the product of the covering fraction times the column density estimated from the smallest statistically necessary line.

3. **FC+PL:** The absorber completely covers the continuum emission region, and partially covers the emission-line region. In this case, since the continuum is completely covered, the best estimate of the column density is that estimated from the smallest statistically necessary line (i.e., the covering fraction is 1.)

We can make some inferences about the nature and location of the absorber among the eight objects in which partial covering was statistically necessary. In six spectra, the Hα line was too deep to be consistent with the PC case, i.e., the continuum partially covered and the emission lines uncovered. In fact, the two objects that favored the PC model are the ones with no Hα spectral coverage, and it is possible that the preferred spectral model might be different if Hα had been available. This preference suggests that the absorber lies outside of or is cospatial with the broad line region. On the other hand, five were best fit by the FC+PL model, i.e., the absorber completely covers the continuum, but only partially covered the broad emission line region. This suggests that in most of the objects, the absorber is located at a larger radius than the broad line region, but it is not so distant that the BLR and continuum are unresolved with respect to the unknown structure in absorbing gas that is the origin of partial covering (i.e,. the case required by P(L+C) partial covering).

In three cases, the best-fitting partial covering model did not fit as well as the unconstrained model, i.e., the unphysical one in which all absorption line optical depths are allowed to vary independently. The best-fitting unconstrained and partial covering models for SDSS J1635+1439 are shown in Fig. 2. The Balmer absorption apparent optical depth in this object is the largest in the sample, but the simple step-function partial covering mdoel is not consistent with the shape of the Hα absorption

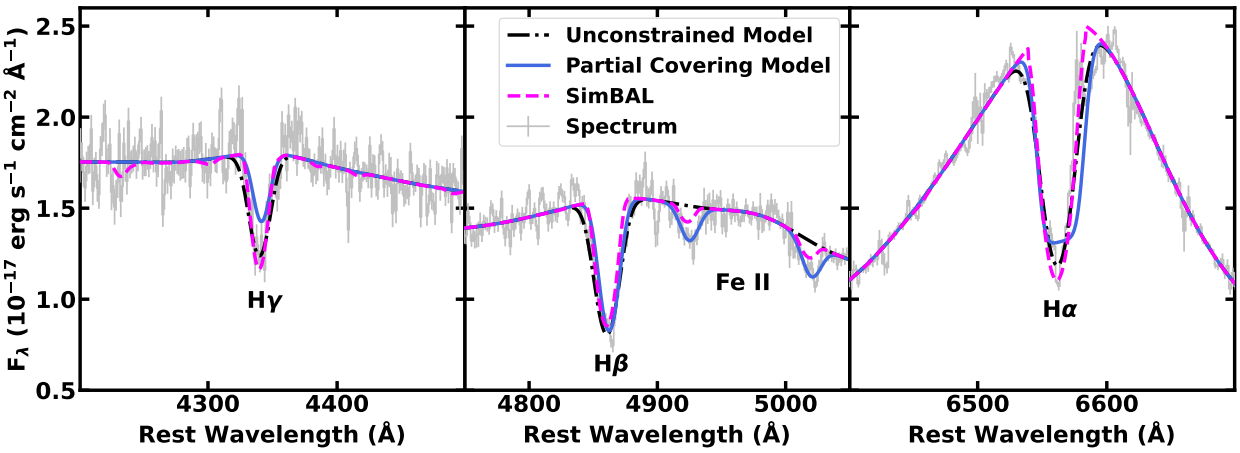

Figure 2. An illustration of partial covering models in SDSS 1635+1439. The black line shows the unconstrained model fit in which the relative Balmer optical depths were allowed to vary independently, yielding an excellent fit but an unphysical model. The blue line shows the best-fitting step-function partial covering model. The Hα line is truncated because the absorption on the continuum is saturated and it is not black because the partially-covered BLR fills it in. The magenta line shows an illustration of a `SimBAL` model. `SimBAL` uses power-law partial covering (e.g., K. M. Leighly et al. 2018, 2019), which allows the line to largely retain its shape and yields an overall better fit. We note that this is not formal a `SimBAL` model fit; those will be presented in Choi et al. in prep.

line. A more complex model such as the power-law partial covering model (e.g., M. de Kool et al. 2002; B. M. Sabra & F. Hamann 2005; N. Arav et al. 2005), in which $\tau(x) = \tau_{max} x^a$ where x is the fractional surface area, may be justified. Fig. 2 shows an example of a `SimBAL` model[11] overlaid on the partial covering model for the purpose of illustration. The power-law partial covering model both fits the line ratios better (especially Hγ), and it also retains the shape of Hα better.

Along with the optical depth measurements (i.e., the maximum optical depth, the apparent column density of Hα, and the true column density estimate that takes into account the partial covering) given in Table 2, we computed three measures of dN/dv, i.e., the optical depth or column density divided by the line FWHM, yielding an approximate measure of the opacity per speed interval. This parameter is motivated if the acceleration mechanism is radiative line driving, as the amount of

[11] We note that this is not a formal `SimBAL` model fit to the broadband spectrum, but rather a by-hand χ-by-eye model fit; the formal `SimBAL` model fit will be included in Choi et al. (in prep.).

radiation absorbed depends on there being sufficient ions present but also that there be a velocity dispersion so that an ion absorbs a wide band of continuum photons rather than the relatively few continuum photons absorbed if the gas is stationary (V. V. Sobolev 1957). The complex BAL spectra which includes absorption from many excited states ensures that sufficient ions are present for the gas to be accelerated by radiative line driving (the dN part), while the width of the line indicates how much of the continuum will be absorbed (the dV part).

3.2. *Accretion Properties*

We followed nearly the same procedure as K. M. Leighly et al. (2022) to estimate the bolometric luminosity, black hole mass, and Eddington ratio, as described below. The values are given in Table 3.

To estimate the bolometric luminosity and black hole mass, we needed measurements of the rest-frame flux density at 5100Å and 3μm. We used a linear interpolation of the log of the flux densities of the nearest larger and smaller wavelength photometry points. To estimate the uncertainty, we repeated the interpolation 10,000 times, perturbing the flux density values using a normal distribution with standard deviation equal to the photometry errors.

As in K. M. Leighly et al. (2022), we estimated the bolometric luminosity using the rest-frame flux density at 3μm and the bolometric correction derived by S. C. Gallagher et al. (2007b). The black hole mass requires an estimate of the radius of the Hβ-emitting broad-line region. As in K. M. Leighly et al. (2022), we used the formalism given by M. C. Bentz et al. (2006). A difference between that paper and this one is that we estimated the luminosity density at 5100Å from the photometry rather than the continuum measurement from spectral fitting because our near-IR spectra are not reliably fluxed. We did not correct for reddening intrinsic to the quasar, noting that the photometry SEDs show that most appear unreddened. The black hole mass was estimated using the FWHM of the Hβ line and following the formalism of S. Collin et al. (2006). In particular, we used their Equation 7 to estimate the scale factor f based on the FWHM of the Hβ line.

α_{oi}, used previously by K. M. Leighly et al. (2024) to characterize the optical–NIR spectral energy distribution, is a measure of both the reddening (the blue half) and the relative strength of the upturn longward of the 1μm dust-sublimation break that is thought to be emission from the hot dust on

Table 3. Accretion Properties

Object Name	log Bolometric Luminosity[a] [erg s^{-1}]	log Black Hole Mass[a] [solar masses]	log $L_{\rm Bol}/L_{\rm Edd}$[a]	α_{oi}
080202.69+140315.1	46.99 ± 0.04	9.4 ± 0.05	-0.52 ± 0.06	-1.43 ± 0.13
083942.11+380526.4	46.95 ± 0.05	9.3 ± 0.05	-1.45 ± 0.06	-1.52 ± -0.14
085910.40+423911.3	46.76 ± 0.02	$9.11^{+0.01}_{-0.008}$	-0.45 ± 0.02	-1.15 ± 0.03
101927.37+022521.3	47.01 ± 0.015	$9.16^{+0.02}_{-0.009}$	-0.25 ± 0.02	-0.93 ± 0.03
112526.12+002901.3	46.29 ± 0.02	8.9 ± 0.025	$-0.71^{+0.009}_{-0.05}$	-1.24 ± 0.03
122933.32+583427.6	47.37 ± 0.04	9.56 ± 0.03	-0.29 ± 0.05	-1.24 ± 0.08
124452.49+583427.6	47.05 ± 0.025	9.19 ± 0.008	-0.24 ± 0.03	-1.00 ± 0.04
143916.28+162858.5	47.14 ± 0.02	9.27 ± 0.015	-0.23 ± 0.03	-0.92 ± 0.04
160915.16+561943.2	46.45 ± 0.02	8.96 ± 0.009	-0.61 ± 0.02	-1.23 ± 0.03
162119.22+081950.7	47.47 ± 0.03	9.22 ± 0.01	0.14 ± 0.03	-0.59 ± 0.05
162527.73+093332.8	47.26 ± 0.03	9.35 ± 0.06	-0.19 ± 0.06	-1.27 ± 0.14
163515.87+143925.9	46.53 ± 0.02	9.22 ± 0.03	-0.79 ± 0.04	-0.94 ± 0.04
164419.75+530750.4	46.39 ± 0.02	9.06 ± 0.09	$-0.77^{+0.09}_{-0.08}$	-1.06 ± 0.05
172341.08+555340.5	47.41 ± 0.02	9.31 ± 0.02	0.00 ± 0.03	-1.28 ± 0.06

[a] Parameter uncertainies are estimated using measurement errors (e.g., uncertainties in flux density or FWHM) only. Systematic errors in single epoch estimates of black hole masses are typically a few tenths dex (e.g., M. Vestergaard & B. M. Peterson 2006).

the inner edge of the torus (the red half)[12]. For reference, the C. M. Krawczyk et al. (2013) quasar composite spectrum yields $\alpha_{oi} = -0.97$.

The bolometric luminosity $L_{\rm Bol}$, the black hole mass, the Eddington ratio, and α_{oi} are given in Table 3. As before, the uncertainties were generated from the distribution of 10,000 random draws of measurements from perturbed flux values.

[12] In K. M. Leighly et al. (2024), we also estimated $D_{\rm red}$ and $D_{\rm torus}$, measures of the difference between the mean SED from the unabsorbed comparison sample introduced in K. M. Leighly et al. (2022) on the red side and blue side, respectively. These two parameters break the degeneracy between reddening and torus strength in α_{oi} (Table 1, Fig. 3 in K. M. Leighly et al. 2024, for definitions and discussion). The photometry data used in this paper are not robust enough to estimate $D_{\rm red}$ and $D_{\rm torus}$, chiefly from the lack of observed-frame near-infrared (rest-frame optical) photometry in 7 objects, leaving some ambiguity in how to interprete the α_{oi} results presented here.

4. CORRELATIONS

In order to gain insight into the nature of Balmer absorption in FeLoBAL quasars, we performed a correlation analysis. The Spearman rank correlation is appropriate for these data, since there is no reason to expect that the measurements should have a Gaussian distribution. We represent the results in Fig. 3 in the same way as in K. M. Leighly et al. (2022) and K. M. Leighly et al. (2024). Specifically, the plots represent the log of the p-value for the correlation, where the sign of the value represents the sense of the correlation. For example, a large negative value implies a highly significant anticorrelation. We computed correlations separately for the sample of 12 objects that all have Hα in their spectra separately from the 14 object sample that includes two objects that only have Hβ in their spectra.

As discussed in § 3, the column density estimates are uncertain because although there is evidence for partial covering in all objects, the amount and nature of the partial covering is difficult to determine. When partial covering is not taken into account, the column density measurements are a lower limit. In principle, this means that we should use correlation methodology that takes into account lower limits. However, those methods are generally intended for cases when all the data is uniform and the limits arise from detectability, e.g., as in a flux-limited sample. This is not the case for our spectra; in a sense, all of our measurements are limits. Therefore, we do not explicitly take lower limits into account but rather bear these limitations in mind in the analysis. We also plan compare these results with the `SimBAL` modeling results which accounts for the partial covering explicitly using the full spectrum (Choi et al. in prep., Leighly et al. in prep.)

Fig. 3 shows that there are a number of correlations with p values less than our cutoff of 0.05. Many of these are trivial; for example, all measures of optical depth and column density are correlated with one another, and $L_{\rm Bol}$ is correlated with $L_{\rm Bol}/{\rm L_{Edd}}$. Because the sample is small, it is possible that some of these correlations are accidental. We therefore counted a correlation as significant only if correlations of all combinations of samples obtained by taking one object out satisfy our $p < 0.05$ significance criterion (hence referred to as the one-out criterion). These correlations are marked with white stars in Fig. 3 and discussed below.

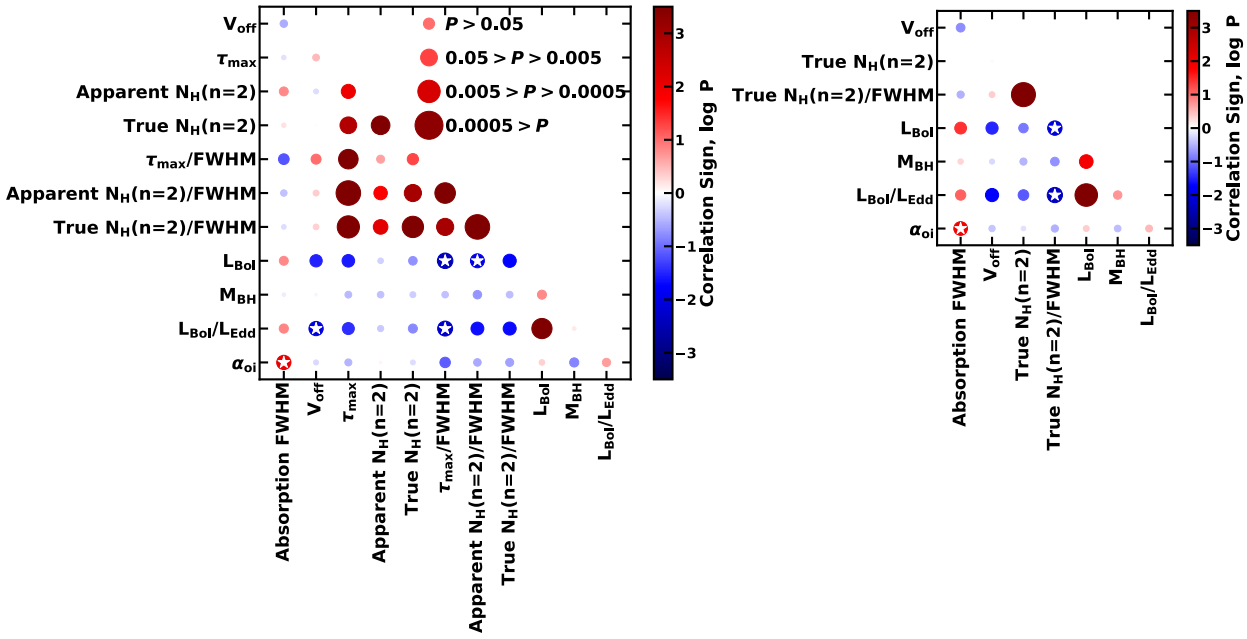

Figure 3. The results of the Spearman rank correlation analysis for the 12-object subsample that covers Hα (left), and for the full 14-object sample (right). The size and color of each marker indicate the sign and p value of the correlation. Anticorrelations are shown in blue, and correlations are shown in red. The shade of the color of each point indicates the significance of the correlation as a continuous variable, while the discrete sizes of the points characterize a range of p values: $p > 0.05$, $0.05 > p > 0.005$, $0.005 > p > 0.0005$, and $0.0005 > p$. The circular markers show the results for the full sample. Most of the strongest positive correlations are trivial, including those between measures of opacity, and $L_{\rm bol}$ versus the Eddington ratio. The stars mark the physically interesting correlations that survive the one-out criterion (see text for details).

4.1. *Correlation between $L_{\rm Bol}$ and Eddington Ratio with $V_{\rm off}$*

We found a significant anticorrelation between the velocity offset and Eddington ratio for the 12 object sample (Fig. 4). The 14 object sample just misses our cutoff with three of the one-out correlations having $p = 0.055$. The anticorrelation between $V_{\rm off}$ and $L_{\rm Bol}$ did not survive the one-out criterion imposed above, but because $L_{\rm Bol}$ and Eddington ratio are strongly correlated, it might be safe to assume that this correlation is present as well.

The anticorrelation between $V_{\rm off}$ and $L_{\rm Bol}$ is ubiquitous among BAL quasars. A. Laor & W. N. Brandt (2002) and R. Ganguly et al. (2007) found that the behavior is more like an upper limit

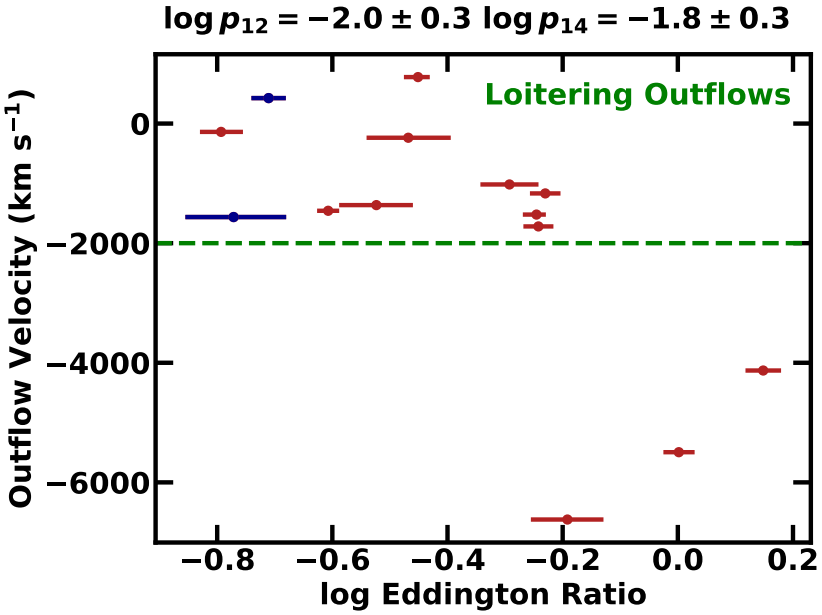

Figure 4. The anticorrelation between Eddington ratio and velocity offset. The red points mark objects that have Hα in the bandpass; the velocity offset is measured from Hβ for the two objects with blue points. The p values included above the plot were computed for the 12-member sample that includes Hα in the spectrum (p_{12}) and the full sample (p_{14}). The anticorrelation is common among BAL quasars but is weak in this sample, most likely because most of the targets belong to the loitering outflow class (above the green dashed line). First identified by H. Choi et al. (2022b), loitering outflow quasars are identified by their low outflow speeds and compact outflows.

envelope so that a quasar needs to have a certain luminosity to attain a very large outflow velocity, but lower velocities are also observed. H. Choi et al. (2022b) found a correlation between $L_{\rm Bol}$ and velocity offset among low-redshift FeLoBAL quasars.

In our case, the anticorrelation is not very strong, and examination of Fig. 4 shows why. Eleven of of the fourteen objects that show Balmer absorption are loitering outflow FeLoBAL quasars. This class of objects was first identified by H. Choi et al. (2022b, see their Fig. 18). Specifically, H. Choi et al. (2022b) found that most of the low-redshift FeLoBAL quasars show an anticorrelation between the outflow location and the outflow speed such that outflows located close to the central engine have the highest outflow speeds. (This is the behavior expected if the outflows are accelerated by radiative line driving, because the radiation flux is largest close to the central engine.) The loitering

outflow FeLoBALQs are were identified as outliers from this relationship with $\log R < 1$ [pc] and $|V_{\rm off}| < 2000\,{\rm km\,s^{-1}}$, i.e., very low outflow speeds for their location close to the central engine. While we do not yet have the `SimBAL` measurements of $\log R$ for the high-redshift FeLoBAL sample, and we expect that the criterion will scale with luminosity (i.e., the criterion may be better expressed as in terms of $\log R/R_{\rm sub}$, where $R_{\rm sub}$ is the dust sublimation radius), we can confirm that nearly all of the objects in our sample have the Fe II absorption morphology typical of a loitering outflow; specifically, strong absorption from highly-excited states. Thus the correlation seen in this sample is essentially between the the loitering outflow candidates, which have $V_{\rm off} < 2000{\rm km\,s^{-1}}$, and the three objects with larger velocities: SDSS J1621+0819, SDSS J1625+0933, and SDSS J1723+5553. Of these three, only SDSS J1723+5553 has Fe II absorption morphology more typical of an ordinary FeLoBALQ; the other two show the strong highly-excited-state Fe II absorption characteristic of loitering BAL outflows. In other words, we cannot expect strong correlations with outflow velocity in a sample dominated by a type of object that is characterized by a limited range of outflow velocities.

We note that the fact that nearly all of these objects are loitering outflow FeLoBALQs is consistent with the result from §3.1 that most of the objects in which partial covering could be detected are best fit by the FC+PL model. `SimBAL` model fitting results of loitering outflow FeLoBALQs generally find a location near the torus, consistent with the partial covering results, i.e., close enough that the angular size of the broadline region is resolved, but the angular size of the continuum emitting region is not (for further discussion, see K. M. Leighly et al. 2019; H. Choi et al. 2022a).

4.2. *Correlations between dN/dv Measures and Eddington Ratio*

We found that $L_{\rm Bol}$ and the Eddington ratio are anticorrelated with several measures of the differential line opacity such that higher values of dN/dv are found in objects with lower outflow velocity widths. Five such correlations among the 12 and 14 object samples survive the one-out correlation criterion; Fig. 5 shows one of them. Fig. 5 also shows the Hα profiles for the sample. Despite the fact that this plot only shows the apparent optical depth profile and partial covering is not taken into account, it gives the general impression that higher velocity outflows tend to be both shallower and broader.

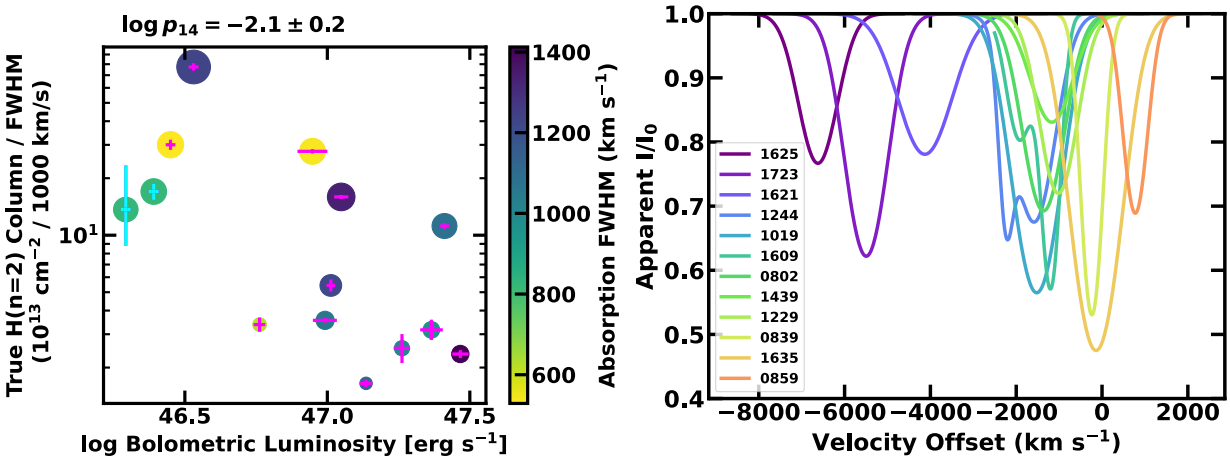

Figure 5. *Left:* An example of one of the anticorrelations between measures of dN/dv and $L_{\rm Bol}$ or Eddington ratio. The log of the significance for this correlation is given at the top of the plot. The circular marker color indicates the absorption line FWHM, which is weakly correlated with $L_{\rm Bol}$, while the circular marker size indicates the log of the true column density, which is weakly anticorrelated with $L_{\rm Bol}$. The errors on the parameters are shown in pink and cyan for the two objects that lack Hα observations. *Right:* The twelve Hα absorption profiles labeled by their RAs in inverse order of outflow speed. There is a general trend for higher velocity lines to be shallower and possibly broader.

Among the interesting correlations marked with stars in Fig. 3, we found stronger correlations among the dN/dv measures than the integrated opacity measures. Because dN/dv is a ratio, we can ask whether the anticorrelation arises from an anticorrelation between column density and $L_{\rm Bol}$, and/or a correlation between FWHM and $L_{\rm Bol}$ (likewise between these two parameters and Eddington ratio). As shown in Fig. 3, both relationships are present, although they are weak; only FWHM versus $L_{\rm Bol}$ satisfies our $p < 0.05$ criterion, while the others range from $0.085 < p < 0.18$. The dependence on these two parameters is illustrated in Fig. 5 by the colorbar and symbol size, respectively.

4.3. *Correlation between α_{oi} and Absorption Line FWHM*

The final correlation that survived the one-out criterion is the positive correlation between α_{oi} and absorption line FWHM shown in Fig. 6.

α_{oi} was a key parameter in the analysis of low-redshift FeLoBAL quasars presented by K. M. Leighly et al. (2024). As noted above, α_{oi} simultaneously measures reddening and the strength of the torus

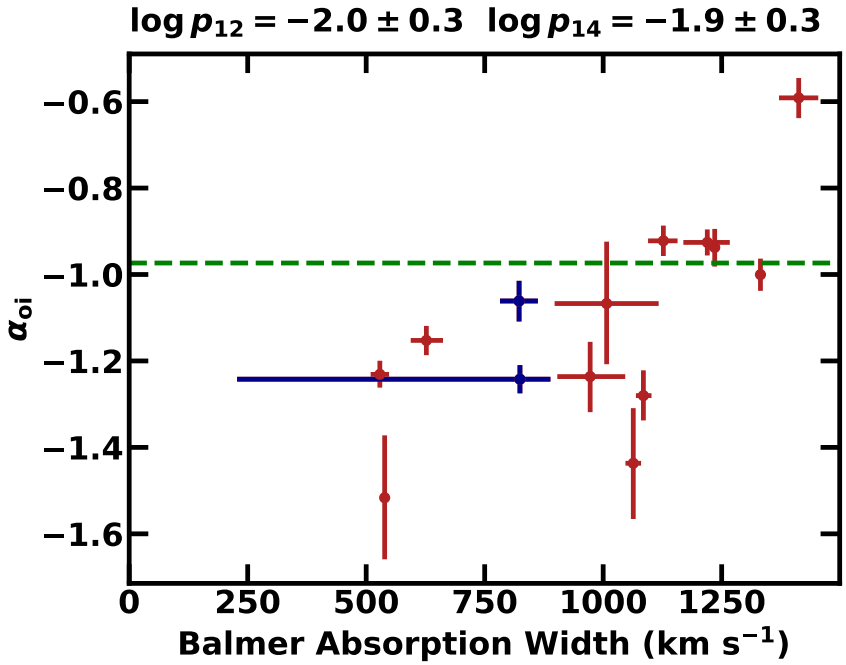

Figure 6. Relationship between the absorption line width and $\alpha_{\rm oi}$, the point-to-point slope between 5100Å and 3μm. The red points mark objects that have Hα in the bandpass; the velocity offset is measured from Hβ for the two objects with blue points. The horizontal line marks the α_{oi} value from the C. M. Krawczyk et al. (2013) composite spectrum. Objects with values near or below this line have no reddening and weak torus emission. The object with the large value of α_{oi} is SDSS 1621+0819, and the value is large due to a large flux in *WISE* W3, with signal-to-noise ratio of 13.9.

(see Fig. 3 in K. M. Leighly et al. 2024), with larger (i.e., more positve and flatter) values indicating stronger reddening and stronger torus emission. In that analysis, α_{oi} was strongly anticorrelated with the location of the outflow, but among the unabsorbed comparison sample, it was also strongly correlated with the Eddington ratio and black hole mass (see Fig. 11 in K. M. Leighly et al. 2024) such that objects with higher accretion rates showed large (more positive and therefore flatter) values of α_{oi}. Because the unabsorbed comparison objects showed little evidence for reddening (Fig. 4 in K. M. Leighly et al. 2024), these larger values correspond stronger hot dust emission. α_{oi} was also correlated with $R_{\rm FeII}$, the ratio of the optical Fe II emission to the Hβ emission. This ratio is broadly thought to be related to quasar fundamental physical parameters such as black hole mass, accretion rate, and orientation (e.g., Y. Shen & L. C. Ho 2014). Thus, it could be that the correlation observed

in this sample is a side effect of the anticorrelation between Eddington ratio and outflow velocity discussed above.

It is notable that in this sample, nearly all objects have α_{oi} values steeper than the quasar SED composite spectrum from C. M. Krawczyk et al. (2013). This behavior was also found among the low-redshift loitering outflows (K. M. Leighly et al. 2024, Fig. 13). Specifically, the SEDs of those objects (with nore negative α_{oi} values) were consistent with no reddening and notably weak torus emission. In K. M. Leighly et al. (2024) we linked the weak torus emission to the low accretion rate typical of loitering outflow objects (§8.1) of that paper. The lack of reddening among the loitering outflow FeLoBAL quasars contrasts with the general trend that BALQs tend to be reddened compared with unabsorbed quasars (e.g., C. M. Krawczyk et al. 2015).

5. DISCUSSION

5.1. *Population Properties*

Balmer absorption is rare among FeLoBAL quasars, and even rarer among the general population of quasars. Studying the properties of extreme objects can give us valuable insight into the phenomenon in general; such a study is even more valuable when a sample of such objects can be studied. Previously, the literature on Balmer absorption consisted of reports of the phenomenon in one or two objects. Given the rarity of examples of Balmer absorption lines observed in quasar spectra, this sample of 14 objects is a significant addition to the literature and reveals important insights into this class of quasar outflows.

Nearly all of the objects with Hβ absorption lines are classified as loitering outflow FeLoBALQs. As outlined above, H. Choi et al. (2022b) developed this class to describe objects with compact, low-velocity outflows that were outliers from the radius and outflow speed anticorrelation exhibited by most of the FeLoBAL quasars (H. Choi et al. 2022b, Fig. 18). K. M. Leighly et al. (2022) found that low-redshift FeLoBAL quasars were characterized by either a low accretion rate or a high accretion rate, while intermediate accretion rates more typical of an unabsorbed quasars were not observed. The loitering outflow quasars in those papers were all members of the low accretion rate group,

which had a median Eddington ratio of ($\log L_{\rm Bol}/L_{\rm Edd} = -0.95$). The median Eddington ratio of this sample is higher ($\log L_{\rm Bol}/L_{\rm Edd} = -0.37$). However, that difference is likely to be a consequence of the flux limited nature of SDSS, and observational feasibility. Low-accretion-rate objects produce less light and are predicted to fall out of flux-limited samples at higher redshifts (S. Jester et al. 2005), which means that high-redshift loitering outflow FeLoBALQs are even rarer in SDSS than are the lower-redshift ones. In addition, they needed to be bright enough to obtain NIR spectra of sufficient SNR on $<$ 8-meter class telescopes in a reasonable amount of time.

Another hallmark of a low accretion rate is broad Balmer emission lines, strong [O III], and weak Fe II (e.g., Y. Shen & L. C. Ho 2014). K. M. Leighly et al. (2022) found these signatures among the low accretion rate FeLoBAL quasars (Fig. 9 in that paper). While some of the spectra shown in Fig. 1 have strong [O III] (e.g., SDSS 0859+4239, SDSS 1019+0225; see also A. Schulze et al. 2018), others do not. However, [O III] is known to show a particularly strong Baldwin effect (e.g., H. Netzer et al. 2004; D. Stern et al. 2012; B. Wang et al. 2025), so we can expect weaker [O III] emission lines in a higher-redshift (and therefore higher luminosity) sample. Whether or not there are detectable differences among the optical emission lines in our high-redshift FeLoBALQ sample will have to wait for analysis of the remainder of the sample and the unabsorbed comparison sample (Leighly et al. in prep.).

As mentioned above, H. Choi et al. (2022b) used `SimBAL` to extrapolate the best spectral models for our sample of low-redshift FeLoBAL quasars to the rest-frame optical band to predict the presence of Balmer absorption (Fig. 16 in that paper). They found that *all* compact outflows ($\log R <\sim 1$ [pc]) predicted significant opacity in Balmer absorption lines. This included the loitering outflow FeLoBALQs, but also the overlapping trough quasars. P. B. Hall et al. (2002) described this class of absorption lines: "the troughs remain deep at velocities comparable to the spacing of absorption troughs from different transitions, so that there are no continuum windows between the troughs." `SimBAL` analysis shows that overlapping FeLoBALQs have the same high-excitation Fe II as the loitering outflows; the difference is that the lines are very broad ($> 4000\,{\rm km\,s^{-1}}$ versus $< 2000\,{\rm km\,s^{-1}}$ for the loitering outflows) so that individual transitions are difficult to identify. Both loitering outflow

and overlapping trough FeLoBALQs have outflows located close to the central engine, but they are strikingly different in other ways. While loitering outflows are characterized by a low accretion rate, overlapping trough quasars are characterized by a high accretion rate (K. M. Leighly et al. 2022). While the speeds of low accretion rate objects increase with radius, the speeds of high accretion rate objects decrease with radius (H. Choi et al. 2022a). Other differences in the structure of the outflows including the volume filling factor are discussed by H. Choi et al. (2022a); specifically, the log volume filling factor was foudn to be between -6 and -4 in most objects, but was as high as -1 for the loitering outflow FeLoBALQs. Our full sample of near-IR spectra from more than 30 FeLoBALQs includes overlapping trough objects, and our preliminary analysis does not reveal any obvious Balmer absorption. One reason that we do not identify Balmer absorption in those spectra that it might be very broad and shallow so that it blends into the continuum. Thus, the sample presented in this paper do not have overlapping trough FeLoBALQs by selection.

5.2. *Implications for BAL Acceleration Mechanisms*

Among the Balmer lines, we found evidence that dN/dv is significantly anticorrelated with Bolometric luminosity and Eddington ratio. This correlation is a consequence of weaker correlations between optical depth (negative) and FWHM (positive) with $L_{\rm Bol}$ and Eddington ratio. We also found that the outflow velocity is correlated with the Eddington ratio.

While the correlation between outflow velocity and bolometric luminosity is a well-known property of BAL quasars (e.g. A. Laor & W. N. Brandt 2002; R. Ganguly et al. 2007), dN/dv is not a parameter that is usually computed, so it is difficult to compare with other studies. However, we observe in our sample that the lines are shallower at higher velocities (Fig. 5), and that is a well-known property of BAL outflows in general. For example, the composite spectra discussed by F. Hamann et al. (2019) clearly illustrate this property, but that is only one of many such studies (see also A. L. Rankine et al. 2020). Although these studies are usually performed on C IV, which is generally saturated so that the column density cannot be estimated from the depth of the trough, the behavior is roughly consistent with expectations from radiative line driving, i.e., it requires much more momentum and energy to accelerate gas to higher velocities.

We can use our Balmer column measurements to roughly examine the behavior of the mass outflow rate and similar properties. The mass outflow rate requires an estimate of the location, the total column density, and the outflow velocity. Because nearly all the objects are loitering outflows, we can assume to zeroth order that they all have nearly the same outflow location. Because Balmer absorption requires extreme physical conditions (i.e., high column density), we can assume that the H(n=2) column density is proportional to the total column density of the outflow. This means that the mass outflow rate, $\dot{M}_{\rm out}$, should be proportional to the product of the outflow speed $|V_{\rm off}|$ and the H(n=2) column density. Likewise, we can compute a momentum flux measure as $\dot{p} \propto |V_{\rm off}|\dot{M}_{\rm out}$, and a kinetic luminosity measure $L_{\rm KE} \propto |V_{\rm off}|\dot{p}$.

We investigated whether these measures are correlated with $L_{\rm Bol}$ and the Eddington ratio. It turns out that there is no correlation between our $\dot{M}$ measure and either $L_{\rm Bol}$ or the Eddington ratio for either the 12-object or the 14-object sample; in each case, $p \sim 0.5$. This behavior arises because $L_{\rm Bol}$ and the Eddington ratio are weakly correlated with the outflow speed (i.e., taken to be positive for an outflow), and weakly anticorrelated with the true $N_{\rm H}$(n=2) column density. This behavior contrasts with the general behavior of quasar outflows, which show a strong correlation between the $L_{\rm Bol}$ and $\dot{M}_{\rm out}$ (e.g., H. Choi et al. 2022b, their Fig. 21). Physically, our result might suggest that $\dot{M}_{\rm out}$ is conserved, and is accelerated to higher velocities when the luminosity and Eddington ratio are increased. However, our $\dot{M}_{\rm out}$ measures span a large range in the sample (a factor of 14), while $L_{\rm Bol}$ and Eddington ratio measurements span only one order of magnitude, so such an interpretation would be overly simplistic. We plan to compare these inferences with the more precise `SimBAL` measurements (Choi et al. in prep.).

In contrast, since $\dot{p}$ and $L_{\rm KE}$ include additional factors of $|V_{\rm off}|$, they are both largely correlated with both $L_{\rm Bol}$ and Eddington ratio ($0.015 < p < 0.059$) in agreement with previous studies (e.g., H. Choi et al. 2022b, and references therein).

5.3. *A Comparison with the Properties of Little Red Dots*

One of the reasons that we decided to present the Balmer absorption line properties in this subsample of near-IR spectra from our high-redshift FeLoBAL quasar sample is because of the recent

discovery of this absorption line in the so-called Little Red Dots (LRDs). While the precise classification of LRDs is under some debate, they are generally taken to be a commonly-found object at $z > 4$ inferred to be an active galaxy from their broad Balmer emission lines (e.g., D. D. Kocevski et al. 2023), although alternative explanations for the broad lines have recently surfaced (e.g., J. F. W. Baggen et al. 2024). Typically, their SED has a V-shape (e.g., D. D. Kocevski et al. 2025). In this section, we compare the properties of Little Red Dots with FeLoBAL quasars, in particular with the loitering outflow FeLoBAL quasars.

5.3.1. *Balmer Absorption Lines*

Balmer absorption lines have been found a number of LRDs (F. D'Eugenio et al. 2025; D. D. Kocevski et al. 2025; J. Matthee et al. 2024). The fraction of LRDs with Balmer absorption has been estimated to be as high as 20% (e.g., K. Inayoshi & R. Maiolino 2025). The Balmer absorption appears in Hα and sometimes Hβ. It is generally narrow (FWHM$\sim 200\,\mathrm{km\,s^{-1}}$) and mildly blueshifted.

It is dangerous to assume an observation phenomenon (Balmer absorption lines) implies a common origin. However, the properties of absorption lines in some LRDs suggest a BAL origin in at least some objects. Metastable helium (He II$*\lambda$10830) absorption has been found in at least one LRD (B. Wang et al. 2025). First reported in a BAL quasar by K. M. Leighly et al. (2011), it is now known to be common among LoBAL quasars (W.-J. Liu et al. 2015), and is predicted to be present in many of the low-redshift FeLoBAL quasars that we studied (H. Choi et al. 2022b). Second, it has been noticed that in LRDs the ratio of the opacity in Hα to Hβ is smaller than required by atomic physics, just like it is in the FeLoBAL quasars presented here. Though this may be evidence for a stellar atmosphere explanation (e.g. F. D'Eugenio et al. 2025), it is possible that partial covering is common in LRDs, just like it is in BAL quasars.

If the origin of the Balmer absorption lines in LRDs is similar to the origin in FeLoBAL quasars, then where is the accompanying FeLoBAL absorption? It may be present but hidden. First, LRDs are defined by a steeply reddened rest-frame optical spectrum. FeLoBAL absorption occurs shortward of Mg IIλ2800 chiefly, so that part of the spectrum may simply be too faint to see Fe II absorption.

Second, LRDs are also found to have a blue spectrum at short wavelengths, which is likely to be a separate component. That separate component may fill in the absorbed and reddened spectrum, making the Fe II absorption lines too shallow to detected (e.g., G. Li et al. 2021).

5.3.2. *Emission Lines*

High-redshift quasars typically have Lorenzian-shaped Balmer lines and strong optical Fe II emission (e.g., M. J. Temple et al. 2024). While LRDs are identified by their broad Balmer emission lines, their emission lines are much different. They tend to have weak or absent Fe II (B. Trefoloni et al. 2024). Their Balmer lines tend to have both a narrow and broad component, i.e., like intermediate-type[13] Seyfert galaxies (e.g., J. Stern & A. Laor 2012). The LRDs are found to have broader Hα lines, and a higher broad-to-narrow Hα ratio than other high redshift Hα selected AGN (A. J. Taylor et al. 2025).

At low redshift, the Fe II, Hβ, and [O III] properties are historically related by a construct known as Eigenvector 1; namely, there is known to be a set of correlations between Fe II and [O III] strengths and Hβ widths that is repeatedly found in rest-frame quasar spectra (e.g., T. A. Boroson & R. F. Green 1992; J. W. Sulentic et al. 2000; D. Grupe 2004; R. R. Ludwig et al. 2009; J. Wolf et al. 2020). This pattern of emission line behavior is further linked with the quasar Eddington ratio (e.g., Y. Shen & L. C. Ho 2014). It was originally thought that BAL quasars were high accretion rate objects, i.e., generally showing strong Fe II and weak [O III], and relatively narrow Balmer lines (T. A. Boroson 2002). However, that scenario was shown to be wrong for low-redshift FeLoBAL quasars by K. M. Leighly et al. (2022). Instead, we found that FeLoBAL quasars were characterized by high and low Eddington ratios, with a lack of objects with intermediate Eddington ratios.

The low-redshift loitering outflow FeLoBAL quasars in K. M. Leighly et al. (2022) are all members of the low accretion rate class. Many of the objects show intermediate-type rest-frame optical spectra; one object was originally classified as a Type 2 quasar (S. Yuan et al. 2016). The composite spectrum

[13] An empirical classification, intermediate-type Seyfert galaxies fall between Seyfert 1 galaxies which have no detectable narrow line region contribution to their Balmer lines, and Seyfert 2 galaxies in which only the narrow line region emission is observed (D. E. Osterbrock 1981).

from the low accretion rate FeLoBAL quasars (K. M. Leighly et al. 2022, Fig. 9) shares the weak Fe II, strong [O III] emission, and intermediate classification characteristic of many LRDs.

On the other hand, the spectra presented in this paper and shown in Fig. 1 are mostly different than those from LRDs. These differences might be attributed to the different ranges of luminosity represented, as many quasar properties are known to be luminosity and accretion rate dependent. First, like X-ray binaries, the configuration of the quasar central engine is believed to change dramatically as the accretion rate is dialed up (e.g., M. Giustini & D. Proga 2019; S. Hagen et al. 2024; P. F. Hopkins 2025). These changes are thought to produce a different broad-band spectral energy distributions, and they may also be accompanied by changes in the broad-line region emission and configuration (e.g., K. M. Leighly 2004, Fig. 15). Second, in flux-limited samples like the SDSS, higher-redshift objects inevitably have higher luminosities, and because the dynamic range of luminosity is larger than that of Eddington ratio, it means that at higher redshift, low accretion rate objects drop out of the sample (S. Jester et al. 2005).

JWST affords the first thorough look at lower-luminosity objects at high redshifts. LRDs have estimated bolometric luminosities between $45 < \log_{10} L_{\rm Bol} < 47$ [erg s^{-1}] (H. B. Akins et al. 2024). The bolometric luminosities of the loitering outflow FeLoBAL quasars in this paper range between $46.3 < \log_{10} L_{\rm Bol} < 47.5$ [erg s^{-1}], i.e., overlapping but higher than many LRDs. However, the low accretion rate FeLoBALs in the low redshift sample presented in K. M. Leighly et al. (2022) range between ~ 45.5 and ~ 46.4, i.e., more typical of the bolometric luminosity estimates for LRDs. We therefore suggest that, to some extent, LRDs have different optical spectra than high-redshift quasars because their luminosity is lower than typical high-redshift quasars.

5.3.3. *Spectral Shape*

One of the characteristic properties of LRDs is that they have a V-shaped spectrum (e.g., D. D. Kocevski et al. 2025), heavily reddened in their rest-frame optical band, with a recovery to a blue spectrum in the near-UV. It is not clear that any of the standard extinction curves satisfactorily model the reddening (e.g., Y. Ma et al. 2025; K. Chen et al. 2025). For example, Z. Li et al. (2025);

Y. Ma et al. (2025) suggested that a deficit of small dust grains, producing a grey extinction curve in the UV, might explain the spectra.

Generally, BAL quasars show stronger reddening and a higher scattering fraction than unabsorbed quasars (e.g., D. Sprayberry & C. B. Foltz 1992; M. S. Brotherton et al. 1997; M. A. DiPompeo et al. 2011; C. M. Krawczyk et al. 2015). Thus their spectra are in some cases also somewhat V-shaped, although they are different in their details from LRDs: BALQ optical spectra can be quite blue at long wavelengths with the steep reddening at shorter wavelengths starting 3000-5000Å, and the recovery to a flat spectrum, when it is present, occurring shortward of $\sim 1800 - 2500$Å (e.g., K. M. Leighly et al. 2009, 2014). The steep reddening curve, known as "anomalous reddening", does not resemble any of the commonly used extinction curves from the Milky Way or Magellanic clouds (e.g. J. A. Cardelli et al. 1988; M. L. Prevot et al. 1984); rather, the curves are very steep through near-UV (P. B. Hall et al. 2002; K. M. Leighly et al. 2009; J. P. U. Fynbo et al. 2013; P. Jiang et al. 2013; K. M. Leighly et al. 2014; J. K. Krogager et al. 2015; H. Meusinger et al. 2016). Anomalous reddening is rare, but it appears to be more common in FeLoBALQs (six objects among ~ 50 H. Choi et al. 2020, 2022b, require it). In the case of FBQS 1408+3054, the reddening can be modeled well using a lognormal dust distribution with mean and standard deviation of 246 and 0.15 microns respectively (Choi et al. in prep.).

The origin of the blue spectrum shortward of the near UV in LRDs is not known, but at least in some cases it is consistent with scattering (e.g., J. E. Greene et al. 2024). Evidence for scattered light is common in BALQ spectra. BALQs are often strongly polarized in their rest-UV spectra (e.g., P. M. Ogle et al. 1999; M. A. DiPompeo et al. 2010, 2011, 2013a); the polarization properties suggest electron or dust scattering (e.g., B. J. Wills et al. 1992; K. M. Leighly et al. 1997). In addition, it is well known that partial covering is required to explain the observed optical depths BAL quasar spectra (F. Hamann 1998). The origin of partial covering is not known (e.g., K. M. Leighly et al. 2019); in some cases it is likely to arise from the details of the opacity (e.g., K. S. Green et al. 2023), but in others, scattering may be important (e.g., H. Choi et al. 2020, 2022b).

5.3.4. *Hot Dust Emission*

One of the puzzling properties of LRDs the lack of hot dust emission; specifically, the spectral energy distributions do not show the typical flattening longward of one micron due to hot ($T_{\rm dust} \sim 1500\,{\rm K}$) dust emission from the inner edge of the torus (e.g., H. B. Akins et al. 2024; B. Wang et al. 2025; K. Chen et al. 2025).

Luminous high-ionization broad absorption line quasars have spectral energy distributions, including torus emission, indistiguishable from unbsorbed quasars (e.g., S. C. Gallagher et al. 2007a; H. Ahmed et al. 2025). In fact, evidence for stronger torus emission in BALQs compared with unabsorbed quasars has been found in some objects (M. A. DiPompeo et al. 2013b).

K. M. Leighly et al. (2024) studied the hot dust properties in a sample of low-redshift FeLoBAL quasars along with a redshift- and luminosity-matched unabsorbed comparison sample. We found a strong correlation between the Eddington ratio and the strength of the torus emission among the unabsorbed quasars. We also found that the low-redshift loitering outflow objects are significantly weak in hot dust emission. K. M. Leighly et al. (2024) linked these correlations to the predicted behavior of the torus as a function of accretion rate in torus wind models. Specifically, it has been proposed that large-scale dynamical outflows are present in quasars, and the torus may be the portion of the wind that is optically thick enough to both block the view of the central engine in AGN unified models and to thermalize incident radiation into emission in the infrared (e.g., R. D. Blandford & D. G. Payne 1982; A. Konigl & J. F. Kartje 1994; S. C. Gallagher et al. 2015). Building upon this idea, M. Elitzur & I. Shlosman (2006) suggested that the torus should disappear at low enough accretion rates that the optically thick wind cannot be sustained. M. Elitzur & L. C. Ho (2009) take these ideas one step further, suggesting that at sufficiently low accretion rates, the broad-line region should disappear. K. M. Leighly et al. (2024) notes that there is substantial evidence in the literature that low-accretion-rate active galaxies lack a torus and may also lack a broad-line region (see § 8.1 in that paper).

5.3.5. *X-ray Properties*

LRDs have been observed to be X-ray weak (e.g., H. B. Akins et al. 2024; B. Wang et al. 2025; M. Yue et al. 2024; D. D. Kocevski et al. 2025). A few objects have been X-ray detected, and their X-ray spectra reveal moderate column densities (e.g., D. D. Kocevski et al. 2025).

BAL quasars are known to be generally X-ray weak (e.g., P. J. Green et al. 2001). Among high-ionization broad absorption line quasars, X-ray spectral analysis generally shows evidence for X-ray absorption; correcting the spectra for this absorption often recovers a normal UV-to-X-ray flux ratio (S. C. Gallagher et al. 2002, 2006). However, some special classes BAL quasars have minimal X-ray absorption (e.g., M. S. Brotherton et al. 2005; M. Giustini et al. 2008; B. P. Miller et al. 2009; R. R. Gibson et al. 2009a), while LoBAL quasars and FeLoBAL quasars have more X-ray absorption (P. J. Green et al. 2001; S. C. Gallagher et al. 2006; L. K. Morabito et al. 2011). Hard X-ray observations of some BAL quasars show them to be intrinsically X-ray weak (B. Luo et al. 2013, 2014). Intrinsic X-ray weakness was also found in the bright, nearby quasar PHL 1811; the X-ray weakness was attributed to the lack of an X-ray emitting corona (K. M. Leighly et al. 2007). Such intrinsic X-ray weakness has been found among JWST AGN, and a similar explanation posited (R. Maiolino et al. 2025).

6. SUMMARY AND CONCLUSIONS

We presented analysis of a sample of 14 FeLoBAL quasars that exhibit Balmer absorption in their rest-frame optical spectra. These include a 9-object subsample from our near-infrared spectroscopic observations of high-redshift (0.97–2.58) FeLoBALQs, supplemented by one archival observation, two spectra from the literature, and two spectra from the SDSS that don't cover Hα but do show Hβ absorption. Eight of these spectra reveal new detections of Balmer absorption lines. Using spectral fitting (Fig. 1), we extracted the offset velocity, velocity width, and optical depth of the Balmer absorption lines. We computed the apparent H(n=2) column density. Taking account of partial covering and the wide range of signal-to-noise ratios of our spectra, we also estimated the true column density (Table 2). We estimated the quasar accretion properties including the black

hole mass, bolometric luminosity, and Eddington ratio. Finally, we estimated α_{oi}, the point-to-point slope between 5100Å and 3μm (Table 3).

We performed a correlation analysis among the measured parameters (Fig. 3). We found an anticorrelation between Eddington ratio and outflow velocity (Fig. 4). Generally found among BAL quasars, the correlation is weak in this sample because nearly all objects are loitering outflow FeLoBAL quasars (H. Choi et al. 2022b), identified by their low outflow velocity and compact absorption. We found anticorrelations between $L_{\rm Bol}$ or Eddington ratio and various computed parameters measuring dN/dv, i.e., the column density per unit velocity (Fig. 5). Finally, we found a correlation between α_{oi} and the absorption velocity width (Fig. 6).

We discussed the implications of these results on our understanding of FeLoBAL quasars (§ 5.1). Among low-redshift FeLoBAL quasars, H. Choi et al. (2022b) predicted that nearly all objects with compact ($\log R < 1\,[\rm pc]$) outflows should have Balmer absorption lines, including both loitering outflow FeLoBALQs and overlapping trough quasars, distinguishable by their dramatically different kinematics. In this paper, we presented only the objects that show Balmer absorption; this criterion includes all the loitering outflow objects, but excludes all the overlapping trough objects, likely because their absorption troughs are so broad that the absorption blends into the continuum. Thus, there is an important selection effect influencing the detectability of Balmer absorption.

Assuming that the outflow location and total column density are the same for all of the detected objects, we computed measures proportional to the mass outflow rate $\dot{M}_{\rm out}$, momentum flux $\dot{p}$, and kinetic luminosity $L_{\rm KE}$. In contrast with other outflow samples, we found that the mass outflow rate does not depend on $L_{\rm Bol}$ or Eddington ratio, while both $\dot{p}$ and kinetic luminosity $L_{\rm KE}$ are positively correlated. We noted, however, that the spread in $\dot{M}_{\rm out}$ is very large, and we will revisit this result using the `SimBAL` analysis results (Choi et al. in prep.).

Finally, we compared the properties of FeLoBAL quasars with the Little Red Dots, a type of object discovered at high redshift by JWST (§ 5.3). We do not claim that FeLoBAL quasars are a local analog of LRDs, but there are several suggestive similarities that may point to common physical origins of like phenomena. The first is the presence of Balmer absorption (§ 5.3.1). LRDs and

FeLoBAL quasars are essentially the only types of active galaxies that show Balmer absorption, and because the physical conditions for Balmer absorption are so extreme, it is possible that they may be the same in some cases. LRDs do not show FeLoBAL absorption lines, but those could be hidden by the strong reddening and blue short wavelength continuum that is their hallmark.

LRDs are also similar in their emission line properties to the low accretion rate branch of FeLoBALs described by K. M. Leighly et al. (2022) in that they often have intermediate Seyfert class Balmer lines, lack Fe II emission, and have strong [O III] lines, i.e., much different than the typical high-redshift quasar (§ 5.3.2). We suggested that this is a consequence of their lower luminosity compared with high-redshift quasars. We noted the similarities in spectral shape, specifically the steep reddening that might be related to the anomalous reddening observed in some FeLoBALQs, and blue continuum (§ 5.3.3) that, being polarized, has a scattering origin in BALQs. We noted the lack of hot dust in LRDs and loitering outflow FeLoBAL quasars (§ 5.3.4). For FeLoBAL quasars, we have suggested that this is a consequence of their low accretion rate (K. M. Leighly et al. 2024). Finally, we noted that both classes are weak in their X-ray emission (§ 5.3.5).

Observations of a common property in a set of objects does not mean that all objects in that set are in all ways identical. For example, all FeLoBAL quasars have Fe II absorption, but K. M. Leighly et al. (2022) showed that they are divided into high and low accretion rate objects. Likewise, the similarities between loitering outflow FeLoBAL quasars and LRDs does not mean that they are the same. Nevertheless, the patterns discussed in this paper, spanning many observational properties, may offer some clues.

ACKNOWLEDGMENTS

KML acknowledges useful discussion with Chanuntorn Pumpo, Gilberto Garcia, and Jorge Escalera. Support for `SimBAL` development and analysis is provided by NSF Astronomy and Astrophysics Grants No. 1518382, 2006771, and 2007023. S.C.G. acknowledges the support of the Natural Science and Engineering Research Council (RGPIN-2021-04157) and a Western University Research Leadership Chair Award. LKM is grateful for support from UKRI [MR/Y020405/1]

Long before the University of Oklahoma was established, the land on which the University now resides was the traditional home of the “Hasinais” Caddo Nation and “Kirikiris” Wichita & Affiliated Tribes. This land was also once part of the Muscogee Creek and Seminole nations.

We acknowledge this territory once also served as a hunting ground, trade exchange point, and migration route for the Apache, Comanche, Kiowa and Osage nations. Today, 39 federally-recognized Tribal nations dwell in what is now the State of Oklahoma as a result of settler colonial policies designed to assimilate Indigenous peoples.

The University of Oklahoma recognizes the historical connection our university has with its Indigenous community. We acknowledge, honor and respect the diverse Indigenous peoples connected to this land. We fully recognize, support and advocate for the sovereign rights of all of Oklahoma’s 39 tribal nations.

This acknowledgement is aligned with our university’s core value of creating a diverse and inclusive community. It is our institutional responsibility to recognize and acknowledge the people, culture and history that make up our entire OU Community.

Funding for the SDSS and SDSS-II has been provided by the Alfred P. Sloan Foundation, the Participating Institutions, the National Science Foundation, the U.S. Department of Energy, the National Aeronautics and Space Administration, the Japanese Monbukagakusho, the Max Planck Society, and the Higher Education Funding Council for England. The SDSS Web Site is http://www.sdss.org/.

The SDSS is managed by the Astrophysical Research Consortium for the Participating Institutions. The Participating Institutions are the American Museum of Natural History, Astrophysical Institute Potsdam, University of Basel, University of Cambridge, Case Western Reserve University, University of Chicago, Drexel University, Fermilab, the Institute for Advanced Study, the Japan Participation Group, Johns Hopkins University, the Joint Institute for Nuclear Astrophysics, the Kavli Institute for Particle Astrophysics and Cosmology, the Korean Scientist Group, the Chinese Academy of Sciences (LAMOST), Los Alamos National Laboratory, the Max-Planck-Institute for Astronomy (MPIA), the Max-Planck-Institute for Astrophysics (MPA), New Mexico State University, Ohio State University,

University of Pittsburgh, University of Portsmouth, Princeton University, the United States Naval Observatory, and the University of Washington.

Funding for SDSS-III has been provided by the Alfred P. Sloan Foundation, the Participating Institutions, the National Science Foundation, and the U.S. Department of Energy Office of Science. The SDSS-III web site is http://www.sdss3.org/.

SDSS-III is managed by the Astrophysical Research Consortium for the Participating Institutions of the SDSS-III Collaboration including the University of Arizona, the Brazilian Participation Group, Brookhaven National Laboratory, Carnegie Mellon University, University of Florida, the French Participation Group, the German Participation Group, Harvard University, the Instituto de Astrofisica de Canarias, the Michigan State/Notre Dame/JINA Participation Group, Johns Hopkins University, Lawrence Berkeley National Laboratory, Max Planck Institute for Astrophysics, Max Planck Institute for Extraterrestrial Physics, New Mexico State University, New York University, Ohio State University, Pennsylvania State University, University of Portsmouth, Princeton University, the Spanish Participation Group, University of Tokyo, University of Utah, Vanderbilt University, University of Virginia, University of Washington, and Yale University.

AUTHOR CONTRIBUTIONS

Karen Leighly: conceptualization; data curation; formal analysis; funding acquisition; investigation; methodology; project administration; resources; software; visualization; writing – original draft, **Sarah Gallagher:** conceptualization; investigation; writing - review and editing, **Donald Terndrup:** conceptualization; funding acquisition; investigation; software; writing - review and editing, **Hyunseop Choi:** conceptualization; funding acquisition; methodology; resources; software; writing - review and editing. **Julianna R. Voelker:** writing - review and editing. **Gordon Richards:** writing - review and editing. **Leah K. Morabito:** writing - review and editing.

Facilities: Gemini(GNIRS), APO (Triplespec)

Software: Sherpa (A. Siemiginowska et al. 2024), Cloudy (G. J. Ferland et al. 2017), SimBAL (K. M. Leighly et al. 2018), PypeIt (J. Prochaska et al. 2020), Triplespectool (M. C. Cushing et al. 2004; W. D. Vacca et al. 2003)

REFERENCES

Ahmed, H., Gallagher, S. C., Shemmer, O., et al. 2025, ApJ, 985, 207, doi: 10.3847/1538-4357/adca38

Akins, H. B., Casey, C. M., Lambrides, E., et al. 2024, arXiv e-prints, arXiv:2406.10341, doi: 10.48550/arXiv.2406.10341

Aoki, K. 2010, PASJ, 62, 1333, doi: 10.1093/pasj/62.5.1333

Aoki, K., Iwata, I., Ohta, K., et al. 2006, ApJ, 651, 84, doi: 10.1086/507438

Arav, N., Kaastra, J., Kriss, G. A., et al. 2005, ApJ, 620, 665, doi: 10.1086/425560

Baggen, J. F. W., van Dokkum, P., Brammer, G., et al. 2024, ApJL, 977, L13, doi: 10.3847/2041-8213/ad90b8

Baskin, A., Laor, A., & Hamann, F. 2015, MNRAS, 449, 1593, doi: 10.1093/mnras/stv406

Bentz, M. C., Peterson, B. M., Pogge, R. W., Vestergaard, M., & Onken, C. A. 2006, ApJ, 644, 133, doi: 10.1086/503537

Blandford, R. D., & Payne, D. G. 1982, MNRAS, 199, 883, doi: 10.1093/mnras/199.4.883

Blanton, M. R., Bershady, M. A., Abolfathi, B., et al. 2017, AJ, 154, 28, doi: 10.3847/1538-3881/aa7567

Boroson, T. A. 2002, ApJ, 565, 78, doi: 10.1086/324486

Boroson, T. A., & Green, R. F. 1992, ApJS, 80, 109, doi: 10.1086/191661

Brotherton, M. S., Laurent-Muehleisen, S. A., Becker, R. H., et al. 2005, AJ, 130, 2006, doi: 10.1086/496948

Brotherton, M. S., Tran, H. D., van Breugel, W., Dey, A., & Antonucci, R. 1997, ApJL, 487, L113, doi: 10.1086/310898

Cardelli, J. A., Clayton, G. C., & Mathis, J. S. 1988, ApJ, 329, L33

Chambers, K. C., Magnier, E. A., Metcalfe, N., et al. 2016, arXiv e-prints, arXiv:1612.05560, doi: 10.48550/arXiv.1612.05560

Chen, K., Li, Z., Inayoshi, K., & Ho, L. C. 2025, arXiv e-prints, arXiv:2505.22600, doi: 10.48550/arXiv.2505.22600

Choi, H., Leighly, K. M., Dabbieri, C., et al. 2022a, ApJ, 936, 110 (Paper III), doi: 10.3847/1538-4357/ac854c

Choi, H., Leighly, K. M., Terndrup, D. M., et al. 2022b, ApJ, 937, 74 (Paper I), doi: 10.3847/1538-4357/ac61d9

Choi, H., Leighly, K. M., Terndrup, D. M., Gallagher, S. C., & Richards, G. T. 2020, ApJ, 891, 53, doi: 10.3847/1538-4357/ab6f72

Collin, S., Kawaguchi, T., Peterson, B. M., & Vestergaard, M. 2006, A&A, 456, 75, doi: 10.1051/0004-6361:20064878

Cushing, M. C., Vacca, W. D., & Rayner, J. T. 2004, PASP, 116, 362, doi: 10.1086/382907

de Kool, M., Korista, K. T., & Arav, N. 2002, ApJ, 580, 54, doi: 10.1086/343107

D'Eugenio, F., Juodžbalis, I., Ji, X., et al. 2025, arXiv e-prints, arXiv:2506.14870, doi: 10.48550/arXiv.2506.14870

DiPompeo, M. A., Brotherton, M. S., Becker, R. H., et al. 2010, ApJS, 189, 83, doi: 10.1088/0067-0049/189/1/83

DiPompeo, M. A., Brotherton, M. S., & De Breuck, C. 2011, ApJS, 193, 9, doi: 10.1088/0067-0049/193/1/9

DiPompeo, M. A., Brotherton, M. S., & De Breuck, C. 2013a, MNRAS, 428, 1565, doi: 10.1093/mnras/sts137

DiPompeo, M. A., Runnoe, J. C., Brotherton, M. S., & Myers, A. D. 2013b, ApJ, 762, 111, doi: 10.1088/0004-637X/762/2/111

Elias, J. H., Joyce, R. R., Liang, M., et al. 2006a, in Society of Photo-Optical Instrumentation Engineers (SPIE) Conference Series, Vol. 6269, Ground-based and Airborne Instrumentation for Astronomy, ed. I. S. McLean & M. Iye, 62694C, doi: 10.1117/12.671817

Elias, J. H., Rodgers, B., Joyce, R. R., et al. 2006b, in Society of Photo-Optical Instrumentation Engineers (SPIE) Conference Series, Vol. 6269, Ground-based and Airborne Instrumentation for Astronomy, ed. I. S. McLean & M. Iye, 626914, doi: 10.1117/12.671765

Elitzur, M., & Ho, L. C. 2009, ApJL, 701, L91, doi: 10.1088/0004-637X/701/2/L91

Elitzur, M., & Shlosman, I. 2006, ApJL, 648, L101, doi: 10.1086/508158

Farrah, D., Urrutia, T., Lacy, M., et al. 2012, ApJ, 745, 178, doi: 10.1088/0004-637X/745/2/178

Ferland, G. J., Chatzikos, M., Guzmán, F., et al. 2017, RMxAA, 53, 385. https://arxiv.org/abs/1705.10877

Fynbo, J. P. U., Krogager, J. K., Venemans, B., et al. 2013, ApJS, 204, 6, doi: 10.1088/0067-0049/204/1/6

Gallagher, S. C., Brandt, W. N., Chartas, G., & Garmire, G. P. 2002, ApJ, 567, 37, doi: 10.1086/338485

Gallagher, S. C., Brandt, W. N., Chartas, G., et al. 2006, ApJ, 644, 709, doi: 10.1086/503762

Gallagher, S. C., Everett, J. E., Abado, M. M., & Keating, S. K. 2015, MNRAS, 451, 2991, doi: 10.1093/mnras/stv1126

Gallagher, S. C., Hines, D. C., Blaylock, M., et al. 2007a, ApJ, 665, 157, doi: 10.1086/519438

Gallagher, S. C., Richards, G. T., Lacy, M., et al. 2007b, ApJ, 661, 30, doi: 10.1086/513733

Ganguly, R., Brotherton, M. S., Cales, S., et al. 2007, ApJ, 665, 990, doi: 10.1086/519759

Ganguly, R., Eracleous, M., Charlton, J. C., & Churchill, C. W. 1999, AJ, 117, 2594, doi: 10.1086/300882

Gibson, R. R., Brandt, W. N., Gallagher, S. C., & Schneider, D. P. 2009a, ApJ, 696, 924, doi: 10.1088/0004-637X/696/1/924

Gibson, R. R., Jiang, L., Brandt, W. N., et al. 2009b, ApJ, 692, 758, doi: 10.1088/0004-637X/692/1/758

Giustini, M., Cappi, M., & Vignali, C. 2008, A& A, 491, 425, doi: 10.1051/0004-6361:200810363

Giustini, M., & Proga, D. 2019, A&A, 630, A94, doi: 10.1051/0004-6361/201833810

Green, K. S., Gallagher, S. C., Leighly, K. M., et al. 2023, ApJ, 953, 186, doi: 10.3847/1538-4357/ace2c4

Green, P. J., Aldcroft, T. L., Mathur, S., Wilkes, B. J., & Elvis, M. 2001, ApJ, 558, 109, doi: 10.1086/322311

Greene, J. E., Labbe, I., Goulding, A. D., et al. 2024, ApJ, 964, 39, doi: 10.3847/1538-4357/ad1e5f

Grupe, D. 2004, AJ, 127, 1799, doi: 10.1086/382516

Hagen, S., Done, C., Silverman, J. D., et al. 2024, MNRAS, 534, 2803, doi: 10.1093/mnras/stae2272

Hall, P. B. 2007, AJ, 133, 1271, doi: 10.1086/511272

Hall, P. B., Anderson, S. F., Strauss, M. A., et al. 2002, ApJS, 141, 267, doi: 10.1086/340546

Hamann, F. 1998, ApJ, 500, 798, doi: 10.1086/305776

Hamann, F., Herbst, H., Paris, I., & Capellupo, D. 2019, MNRAS, 483, 1808, doi: 10.1093/mnras/sty2900

Hewett, P. C., & Foltz, C. B. 2003, AJ, 125, 1784, doi: 10.1086/368392

Hopkins, P. F. 2025, The Open Journal of Astrophysics, 8, 56, doi: 10.33232/001c.137969

Hutchings, J. B., Crenshaw, D. M., Kraemer, S. B., et al. 2002, AJ, 124, 2543, doi: 10.1086/344080

Inayoshi, K., & Maiolino, R. 2025, ApJL, 980, L27, doi: 10.3847/2041-8213/adaebd

Jester, S., Schneider, D. P., Richards, G. T., et al. 2005, AJ, 130, 873, doi: 10.1086/432466

Ji, T., Wang, T.-G., Zhou, H.-Y., & Wang, H.-Y. 2012, Research in Astronomy and Astrophysics, 12, 369, doi: 10.1088/1674-4527/12/4/002

Jiang, P., Zhou, H., Ji, T., et al. 2013, AJ, 145, 157, doi: 10.1088/0004-6256/145/6/157

Knigge, C., Scaringi, S., Goad, M. R., & Cottis, C. E. 2008, MNRAS, 386, 1426, doi: 10.1111/j.1365-2966.2008.13081.x

Kocevski, D. D., Onoue, M., Inayoshi, K., et al. 2023, ApJL, 954, L4, doi: 10.3847/2041-8213/ace5a0

Kocevski, D. D., Finkelstein, S. L., Barro, G., et al. 2025, ApJ, 986, 126, doi: 10.3847/1538-4357/adbc7d

Konigl, A., & Kartje, J. F. 1994, ApJ, 434, 446, doi: 10.1086/174746

Kovačević, J., Popović, L. Č., & Dimitrijević, M. S. 2010, ApJS, 189, 15, doi: 10.1088/0067-0049/189/1/15

Krawczyk, C. M., Richards, G. T., Gallagher, S. C., et al. 2015, AJ, 149, 203, doi: 10.1088/0004-6256/149/6/203

Krawczyk, C. M., Richards, G. T., Mehta, S. S., et al. 2013, ApJS, 206, 4, doi: 10.1088/0067-0049/206/1/4

Krogager, J. K., Geier, S., Fynbo, J. P. U., et al. 2015, ApJS, 217, 5, doi: 10.1088/0067-0049/217/1/5

Laor, A., & Brandt, W. N. 2002, ApJ, 569, 641, doi: 10.1086/339476

Lawrence, A., Warren, S. J., Almaini, O., et al. 2007, MNRAS, 379, 1599, doi: 10.1111/j.1365-2966.2007.12040.x

Leighly, K. M. 2004, ApJ, 611, 125, doi: 10.1086/422089

Leighly, K. M., Choi, H., DeFrancesco, C., et al. 2022, ApJ, 935, 92 (Paper II), doi: 10.3847/1538-4357/ac7e50

Leighly, K. M., Choi, H., Eracleous, M., et al. 2024, ApJ, 966, 87, doi: 10.3847/1538-4357/ad2f2a

Leighly, K. M., Dietrich, M., & Barber, S. 2011, ApJ, 728, 94

Leighly, K. M., Halpern, J. P., Jenkins, E. B., et al. 2007, ApJ, 663, 103, doi: 10.1086/518017

Leighly, K. M., Hamann, F., Casebeer, D. A., & Grupe, D. 2009, ApJ, 701, 176, doi: 10.1088/0004-637X/701/1/176

Leighly, K. M., Kay, L. E., Wills, B. J., Wills, D., & Grupe, D. 1997, ApJL, 489, L137, doi: 10.1086/316793

Leighly, K. M., Terndrup, D. M., Baron, E., et al. 2014, ApJ, 788, 123, doi: 10.1088/0004-637X/788/2/123

Leighly, K. M., Terndrup, D. M., Gallagher, S. C., Richards, G. T., & Dietrich, M. 2018, ApJ, 866, 7, doi: 10.3847/1538-4357/aadee6

Leighly, K. M., Terndrup, D. M., Lucy, A. B., et al. 2019, ApJ, 879, 27, doi: 10.3847/1538-4357/ab212a

Li, G., Shi, X., Tian, Q., et al. 2021, ApJ, 916, 86, doi: 10.3847/1538-4357/ac06c8

Li, Z., Inayoshi, K., Chen, K., Ichikawa, K., & Ho, L. C. 2025, ApJ, 980, 36, doi: 10.3847/1538-4357/ada5fb

Liu, W.-J., Zhou, H., Ji, T., et al. 2015, ApJS, 217, 11, doi: 10.1088/0067-0049/217/1/11

Lucy, A. B., Leighly, K. M., Terndrup, D. M., Dietrich, M., & Gallagher, S. C. 2014, ApJ, 783, 58, doi: 10.1088/0004-637X/783/1/58

Ludwig, R. R., Wills, B., Greene, J. E., & Robinson, E. L. 2009, ApJ, 706, 995, doi: 10.1088/0004-637X/706/2/995

Luo, B., Brandt, W. N., Alexander, D. M., et al. 2013, ApJ, 772, 153, doi: 10.1088/0004-637X/772/2/153

Luo, B., Brandt, W. N., Alexander, D. M., et al. 2014, ApJ, 794, 70, doi: 10.1088/0004-637X/794/1/70

Ma, Y., Greene, J. E., Setton, D. J., et al. 2025, ApJ, 981, 191, doi: 10.3847/1538-4357/ada613

Maiolino, R., Risaliti, G., Signorini, M., et al. 2025, MNRAS, 538, 1921, doi: 10.1093/mnras/staf359

Matthee, J., Naidu, R. P., Brammer, G., et al. 2024, ApJ, 963, 129, doi: 10.3847/1538-4357/ad2345

Meusinger, H., Schalldach, P., Mirhosseini, A., & Pertermann, F. 2016, A&A, 587, A83, doi: 10.1051/0004-6361/201527277

Miller, B. P., Brandt, W. N., Gibson, R. R., Garmire, G. P., & Shemmer, O. 2009, ApJ, 702, 911, doi: 10.1088/0004-637X/702/2/911

Morabito, L. K., Dai, X., Leighly, K. M., Sivakoff, G. R., & Shankar, F. 2011, ApJ, 737, 46, doi: 10.1088/0004-637X/737/1/46

Netzer, H., Shemmer, O., Maiolino, R., et al. 2004, ApJ, 614, 558, doi: 10.1086/423608

Ogle, P. M., Cohen, M. H., Miller, J. S., et al. 1999, ApJS, 125, 1, doi: 10.1086/313272

Osterbrock, D. E. 1981, ApJ, 249, 462, doi: 10.1086/159306

Prevot, M. L., Lequeux, J., Prevot, L., Maurice, E., & Rocca-Volmerange, B. 1984, A&A, 132, 389

Prochaska, J., Hennawi, J., Westfall, K., et al. 2020, The Journal of Open Source Software, 5, 2308, doi: 10.21105/joss.02308

Rankine, A. L., Hewett, P. C., Banerji, M., & Richards, G. T. 2020, MNRAS, 492, 4553, doi: 10.1093/mnras/staa130

Reichard, T. A., Richards, G. T., Hall, P. B., et al. 2003, AJ, 126, 2594, doi: 10.1086/379293

Sabra, B. M., & Hamann, F. 2001, ApJ, 563, 555, doi: 10.1086/324043

Sabra, B. M., & Hamann, F. 2005, ArXiv Astrophysics e-prints

Savage, B. D., & Sembach, K. R. 1991, ApJ, 379, 245, doi: 10.1086/170498

Schulze, A., Misawa, T., Zuo, W., & Wu, X.-B. 2018, ApJ, 853, 167, doi: 10.3847/1538-4357/aaa7f0

Shen, Y., & Ho, L. C. 2014, Nature, 513, 210, doi: 10.1038/nature13712

Siemiginowska, A., Burke, D., Günther, H. M., et al. 2024, ApJS, 274, 43, doi: 10.3847/1538-4365/ad7bab

Skrutskie, M. F., Cutri, R. M., Stiening, R., et al. 2006, AJ, 131, 1163, doi: 10.1086/498708

Sobolev, V. V. 1957, Soviet Ast., 1, 678

Sprayberry, D., & Foltz, C. B. 1992, ApJ, 390, 39, doi: 10.1086/171257

Stern, D., Assef, R. J., Benford, D. J., et al. 2012, ApJ, 753, 30, doi: 10.1088/0004-637X/753/1/30

Stern, J., & Laor, A. 2012, MNRAS, 426, 2703, doi: 10.1111/j.1365-2966.2012.21772.x

Sulentic, J. W., Marziani, P., & Dultzin-Hacyan, D. 2000, ARA&A, 38, 521, doi: 10.1146/annurev.astro.38.1.521

Taylor, A. J., Finkelstein, S. L., Kocevski, D. D., et al. 2025, ApJ, 986, 165, doi: 10.3847/1538-4357/add15b

Temple, M. J., Rankine, A. L., Banerji, M., et al. 2024, MNRAS, 532, 424, doi: 10.1093/mnras/stae1524

Tolea, A., Krolik, J. H., & Tsvetanov, Z. 2002, ApJL, 578, L31, doi: 10.1086/344563

Trefoloni, B., Ji, X., Maiolino, R., et al. 2024, arXiv e-prints, arXiv:2410.21867, doi: 10.48550/arXiv.2410.21867

Trump, J. R., Hall, P. B., Reichard, T. A., et al. 2006, ApJS, 165, 1, doi: 10.1086/503834

Vacca, W. D., Cushing, M. C., & Rayner, J. T. 2003, PASP, 115, 389, doi: 10.1086/346193

Véron-Cetty, M.-P., Joly, M., & Véron, P. 2004, A&A, 417, 515, doi: 10.1051/0004-6361:20035714

Vestergaard, M., & Peterson, B. M. 2006, ApJ, 641, 689, doi: 10.1086/500572

Voelker, J., Choi, H., Leighly, K., DeFrancesco, C., & Dabbieri, C. 2021, in American Astronomical Society Meeting Abstracts, Vol. 53, American Astronomical Society Meeting Abstracts, 337.10

Wang, B., de Graaff, A., Davies, R. L., et al. 2025, ApJ, 984, 121, doi: 10.3847/1538-4357/adc1ca

Wang, J., & Xu, D. W. 2015, A&A, 573, A15, doi: 10.1051/0004-6361/201424848

Wang, T., Dai, H., & Zhou, H. 2008, ApJ, 674, 668, doi: 10.1086/525242

Wills, B. J., Wills, D., Evans, II, N. J., et al. 1992, ApJ, 400, 96, doi: 10.1086/171976

Wilson, J. C., Henderson, C. P., Herter, T. L., et al. 2004, in Society of Photo-Optical Instrumentation Engineers (SPIE) Conference Series, Vol. 5492, Ground-based Instrumentation for Astronomy, ed. A. F. M. Moorwood & M. Iye, 1295–1305, doi: 10.1117/12.550925

Wolf, J., Salvato, M., Coffey, D., et al. 2020, MNRAS, 492, 3580, doi: 10.1093/mnras/staa018

Wright, E. L., Eisenhardt, P. R. M., Mainzer, A. K., et al. 2010, AJ, 140, 1868, doi: 10.1088/0004-6256/140/6/1868

Yuan, S., Strauss, M. A., & Zakamska, N. L. 2016, MNRAS, 462, 1603, doi: 10.1093/mnras/stw1747

Yue, M., Eilers, A.-C., Ananna, T. T., et al. 2024, ApJL, 974, L26, doi: 10.3847/2041-8213/ad7eba

Zakamska, N. L., & Greene, J. E. 2014, MNRAS, 442, 784, doi: 10.1093/mnras/stu842

Zhang, S., Zhou, H., Shi, X., et al. 2015, ApJ, 815, 113, doi: 10.1088/0004-637X/815/2/113